Theses and Dissertations

Theses and Dissertations

5-5-2017

Laser-Induced Breakdown Spectroscopy: Simultaneous Multi-Elemental Analysis and Geological Applications

Herve Keng-ne Sanghapi

Follow this and additional works at: https://scholarsjunction.msstate.edu/td

Laser-induced breakdown spectroscopy: simultaneous multi-elemental analysis and

geological applications

By

Hervé Keng-né Sanghapi

A Dissertation
Submitted to the Faculty of
Mississippi State University
in Partial Fulfillment of the Requirements
for the Degree of Doctor of Philosophy
in Engineering with emphasis in Applied Physics
in the Bagley College of Engineering

Mississippi State, Mississippi

May 2017

Laser-induced breakdown spectroscopy: simultaneous multi-elemental analysis and

geological applications

By

Hervé Keng-né Sanghapi

Approved:

_____
Hendrik F. Arnoldus
(Major Professor)

_____
Jagdish P. Singh
(Director of Dissertation)

_____
David L. Monts
(Committee Member)

_____
Dustin L. McIntyre
(Committee Member)

_____
Kalyan K. Srinivasan
(Committee Member)

_____
Jason M. Keith
Dean
Bagley College of Engineering

Name: Hervé Keng-né Sanghapi

Date of Degree: May 5, 2017

Institution: Mississippi State University

Major Field: Engineering with emphasis in Applied Physics

Director of Dissertation: Jagdish P. Singh

Title of Study: Laser-induced breakdown spectroscopy: simultaneous multi-elemental
                 analysis and geological applications

Pages in Study 112

Candidate for Degree of Doctor of Philosophy

Under high irradiation, a fourth state of matter named plasma can be obtained. Plasmas emit electromagnetic radiation that can be recorded in the form of spectra for spectroscopic elemental analysis. With the advent of lasers in the 1960s, spectroscopists realized that lasers could be used simultaneously as a source of energy and excitation to create plasmas. The use of a laser to ignite a plasma subsequently led to laser-induced breakdown spectroscopy (LIBS), an optical emission spectroscopy capable of analyzing samples in various states (solids, liquids, gases) with minimal sample preparation, rapid feedback, and endowed with *in situ* capability. In this dissertation, studies of LIBS for multi-elemental analysis and geological applications are reported.

LIBS was applied to cosmetic powders for elemental analysis, screening and classification based on the raw material used. Principal component analysis (PCA) and internal standardization were used. The intensity ratios of Mg/Si and Fe/Si observed in talcum powder show that these two ratios could be used as indicators of the potential presence of asbestos.

The feasibility of LIBS for the analysis of gasification slags was investigated and results compared with those of inductively-coupled plasma−optical emission spectrometry (ICP-OES). The limits of detection for Al, Ca, Fe, Si and V were determined. The matrix effect was studied using an internal standard and PLS-R. Apart from V, prediction results were closed to those of ICP-OES with accuracy within 10%.

Elemental characterization of outcrop geological samples from the Marcellus Shale Formation was also carried out. The matrix effect was substantially reduced. The limits of detection obtained for Si, Al, Ti, Mg, Ca and C were determined. The relative errors of LIBS measurements are in the range of 1.7 to 12.6%.

Gate delay and laser pulse energy, have been investigated in view of quantitative analysis of variation of trace elements in a high-pressure environment. Optimization of these parameters permits obtaining underwater plasma emission of calcium with quantitative results on the order of 30 ppm within a certain limit of increased pressure. Monitoring the variation of the trace elements can predict changes in the chemical composition in carbon sequestration reservoir.

DEDICATION

To my parents, Helene and Marc-Aurele Sanghapi. You have been relentless in your efforts and support in seeing me through my education. I hope you find in this work the beginning of more accomplishments than you ever wished for me.

To my sisters, Judith, Sandrine, Axline, Christelle and my brothers Rudolf, Donald and Derick for always being there for me with your unconditional love and care.

To my lovely wife, Geraldine for her patience and prayers.

To my little boy Elnathan Sanghapi, may this work inspire you as you grow up.

To God Almighty, whom through His Son Jesus Christ, has given me the Grace to finalize my dissertation.

ACKNOWLEDGEMENTS

I am forever grateful to Mississippi State University and particularly to the Department of Physics and Astronomy for granting me a Graduate Teaching Assistantship for my studies. Without their admission offer, this would not have been possible.

Last but not the least, my sincere gratitude to the Oak Ridge Institute for Science and Education (ORISE) for offering a postgraduate fellowship which gave me the opportunity to acquire professional and experimental training beyond the four walls of a classroom. It was quite a challenge and very enriching.

TABLE OF CONTENTS

LIST OF TABLES

LIST OF FIGURES

CHAPTER I

INTRODUCTION

Atomic emission spectroscopy (AES) has been long used by spectroscopists for multi-elemental analysis of material samples which could be solid, liquid or gaseous samples [1]. In a nutshell, under excitation, electromagnetic radiation emitted by matter is measured in the form of spectra which are then analyzed in order to obtain qualitative (identify the elements in the sample) or quantitative (relative abundance of each element) results. The quality of these results greatly depends on the source of excitation. In effect, the excitation source has led to various techniques of atomic emission spectroscopy with much success. Although early sources of spectra, such as flames, arcs, and sparks, laid down the foundation of spectrochemistry, plasma is now widely used. We can include microwave-induced plasmas (MIP), direct current plasmas (DCP), and inductively-coupled plasmas (ICP) [2]. The most remarkable workhorses in atomic emission spectroscopy have been electrode spark and inductively-coupled plasmas with the later having better limits of detection [2][3]. However, these are limited by possible contamination and interferences from the excitation source and by the sample preparation procedure (digestion). The fact that the sample is prepared separately and introduced into the source is also a limitation of the technique in terms of rapidity.

1

Laser-induced breakdown spectroscopy

The advent of pulsed lasers in the early 1960s spurred keen research interest in the spectroscopic community as they began investigating its potential use [4], notably as an alternative source of energy and excitation to create plasmas for direct analysis. It was realized that the high power delivered by lasers could be used to directly vaporize and subsequently ionize samples thus avoiding the contamination from sample preparation involved in conventional inductively-coupled plasmas (ICP). This has an advantage of reducing the analytical time. The use of lasers for igniting plasmas subsequently led to other atomic emission spectroscopy (AES) techniques, such as Laser-Induced Breakdown Spectroscopy (LIBS) which is the topic of this dissertation. In his review article, Radziemski [3] traced the transformation of pulsed lasers into commercial technology and its implication for LIBS. The plasmas obtained from laser shots were for the first time referred to as Laser-Induced Breakdown Spectroscopy (better known in its acronym as LIBS) by Loree and Radziemski in 1981 [4]. Ever since, LIBS has steadfastly grown into a versatile and robust spectrometric analytical technique that could be used for *in situ*, fast and real-time analysis with results comparable with those of conventional inductively-coupled plasma−mass spectrometry (ICP-MS) or ICP−optical emission spectrometry (ICP-OES).

Evolution of laser-induced breakdown spectroscopy

Although the acronym LIBS was used for the first time in 1981, the first studies related to the LIBS technique were reported in 1962 by G.C. Dacey [5] on unpublished work of W.S. Boyle. He had formed luminous plasmas on carbon and iron. However, the plasma obtained was not strong enough due to the use of a non-Q-switched laser which

could not deposit sufficient energy onto the targets. Brech and Cross attempted creating plasmas on surface targets. Despite this novelty, the spectra were often too weak to be considered for analytical purposes. Finally, they used an auxiliary electrical spark to enhance excitation [6]. The abstract of their work which appeared in *Applied Spectroscopy* in 1962 [7][8] is considered as the first demonstration of a laser-induced plasma on a solid surface. The first analytical use of lasers for spectrochemical analysis of surfaces was reported in 1963 by Debras-Guédon and Liodec [9] using a ruby laser with optimized conditions for spectral acquisition. Along with the 25 elements detected by LIBS for the first time, the presence of molecular bands, notably AlO and CN, were also observed in the plasma. The elements they could not detect were due to low sensitivity in the ultraviolet region and to the low signal-to-background, attributed to the large unavoidable continuum emission [6]. Debras-Guédon and Liodec also published quantitative studies on determination of Cr and Ni in steel [10]. So far, most experiments used electrical sparks. The advent of improved Q-switched lasers made it possible to directly induce plasmas without electrode excitation [11]. This marked a turning point in LIBS. In 1964, using a pulsed Q-switched laser for direct plasma excitation of metals, Runge *et al.* [12] published the first LIBS calibration curves for Ni and Cr.

By the 1970s, LIBS had interested many researchers across many disciplines, such as mineralogy, geology, metallurgy, archaeology, biology, medicine and forensic science; and the first book written on the subject, by Moenke, was published [13]. The first instruments were developed and commercialized by VEB Carl Zeiss (LMA 1) in Germany, Jarrell-Ash (Model45) in USA and LOMO (MSL-2) in Leningrad. Although promising, results were less impressive than those of other established AES methods, this

3

was mainly due to the quality of the instruments. This resulted in a slow progress within spectroscopic community while fundamental research on characteristics of laser plasmas continue to this day.

The appellation, Laser Induced-Breakdown Spectroscopy (LIBS), by Radziemski and Cremers at Los Alamos National Laboratory in 1981 to describe the breakdown of air using a pulsed laser to create plasmas, is considered as a new beginning of this analytical technique. Since then, research and publications have increased year after year. On one hand, this new interest can be attributed to the need of new analytical methods for certain conditions, such as online analysis, environmental monitoring, and harsh environments not feasible with current methods. On the other hand, compact and ruggedized LIBS systems for field applications have been made feasible with the recent development of optical instruments. Spectrometers with improved spectral resolution and more sensitive detectors and the development of intensified (and recently electron multiplying) charge-coupled device -ICCD (EMCCD) detectors have been introduced as well as more compact and robust lasers.

Significant projects have been accomplished with LIBS, such as the Chemcam on the Curiosity rover on Mars that uses Laser-Induced Breakdown Spectroscopy to provide the elemental composition of soils and rocks on the surface of Mars. Major investigations were to classify rocks using spectral libraries, evaluate sample heterogeneity, depth profiles in the rocks, identify possible organic materials through the detection of C, C_2 or CN molecular bands, identify water on surfaces via weak OH molecular band, and detect hazardous elements, such as Cd, As, Pb and Be [14].

Since 2000, the latest developments of LIBS are often discussed in conferences and symposiums such as:

- International Conference on LIBS.

- The North American Society for Laser-Induced Breakdown Spectroscopy (NASLIBS).

- Euro-Mediterranean Symposium on Laser-Induced Breakdown Spectroscopy (EMSLIBS).

Theoretical background of laser-induced breakdown spectroscopy

Before looking into the theoretical background of LIBS, let us first trace the origin of the word "plasma." Plasma is commonly known as the fourth state of matter. Its origin can be traced back to Irving Langmuir and his works on ionized gases. In 1928 while studying ionized gases, momentum transport due to electrostatic forces made him think of the way blood plasma carried red and white cells. He then related the motion in blood plasma to that of high velocity electrons, ions and impurities in an ionized gas and used the word plasma to describe this region containing balanced charges of ions and electrons [15].

A plasma can be created by the interaction of the laser pulse and the sample which causes breakdown in the material above an irradiance threshold (typically about 1 GW/cm^2) that depends on the material. Although creating a laser-induced plasma seems simple, the mechanism behind it is, however, a series of complex physical processes, consisting of several steps, which we can roughly group into:

- Laser   interaction with sample

- Laser ablation (removal of small amount of sample)

- Breakdown (plasma formation)

5

Plasma formation can be described as shown in Figure1.1
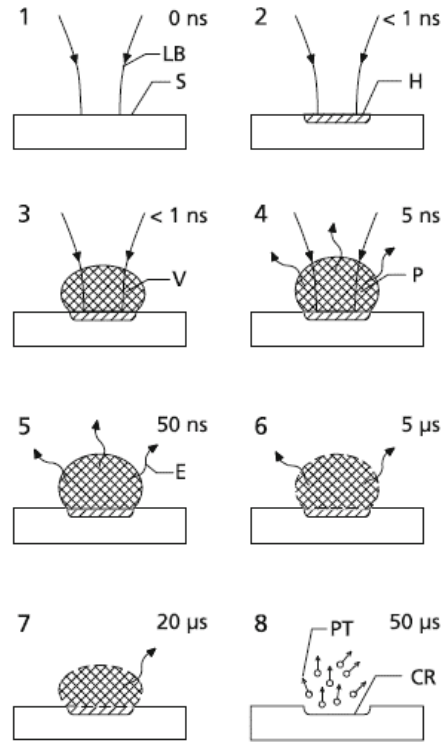
Figure 1.1   Phases of plasma formation in LIBS

LB=incoming laser beam, S=sample, H=region of energy deposition, V=material vapor,
P=plasma, E=element-specific emission, CR=crater, PT=particles.
Adapted from *Laser-Induced Breakdown Spectroscopy, Fundamentals and Applications*
by Reinhard Noll [16].

In Figure 1.1, the various steps of plasma creation are shown. Firstly, in (1) the

surface of the sample is irradiated by a laser pulse. In (2), some of the laser energy is

coupled into the sample material. (3) Above the irradiation threshold of the sample, the

material starts to evaporate. (4) A plasma is ignited, followed by excitation of the

sample's constituents which begin to emit spontaneous radiation. From (5) to (7), the

generated plasma decays and emits element-specific radiation representative of the

elements present in the initial material. (8) At the end of the laser pulse and creation of

6

plasma, a small sample is removed and a small crated is formed in the case of solid substances.

Fundamental notions and theoretical background of laser-induced breakdown spectroscopy can be explained from the theory of plasma physics, which is out of the scope of this dissertation. However, for this experimental work, we will circumscribe our attention only to the mechanisms of generating a LIBS plasma which is known as laser ablation.

Laser ablation

Laser ablation is the main step through which a plasma is generated and the analytical figures of merit of LIBS (when using LIBS with solid target) depend largely on this step. According to Russo, the name "laser ablation" is just a generic name to describe the explosion that occurs during laser-material interaction, which is a more appropriate definition that does not imply a mechanism [17]. Laser ablation is the use of a pulsed laser to remove material from a target sample through more or less complex physical processes, such as melting, fusion, sublimation, ionization erosion, and/or explosion [18]. Depending on the laser pulse characteristics, such as energy, wavelength, and pulse duration, and on the physical and chemical properties of the sample, laser ablation removes an amount of sample varying from hundreds of ng to µg [19]. Laser irradiance (energy per unit time and per unit surface area) and laser pulse duration are the most significant parameters and define the nature of mechanism during laser-material interaction. For short pulses, femtosecond (fs) lasers are used and the primary ablation mechanism is Coulombic explosion which is also known as non-thermal melting; whereas for long pulses, nanosecond (ns) lasers are used and characterized by thermal

mechanisms (melting, sublimation, and vaporization). In between femtosecond and nanosecond lasers, there are picosecond lasers whose ablation mechanism could be both thermal and/or non-thermal [18].

Advantages of short-pulse femtosecond lasers over nanosecond lasers have been reported in several studies. Eland *et al.* [20][21] and Russo *et al.* [22] showed that short pulsed lasers have high precision of sample ablation, lower continuum background, and faster plasma dissipation as compared to nanosecond lasers. When a femtosecond laser is used, the non-interaction of laser radiation with plasma minimizes background emission; coupled to the faster plasma dissipation, temporal resolution of the plasma is not needed for these short laser pulses when associated with high laser pulse rates [20][21][22]. Ablation efficiency with femto-, pico- and nanosecond pulses has been compared as well. At atmospheric pressure, the best efficiency was observed for a femtosecond laser [23] [24].

Most LIBS experiments are done with nanosecond neodymium: yttrium aluminum garnate (Nd: YAG) lasers. Femtosecond and picosecond ablations are extensively discussed in [18]. For the work presented in this dissertation, a nanosecond pulsed laser was used.

Nanosecond ablation

The duration of the laser pulse plays a crucial part in ablating material. Comparing its duration to the characteristic lattice vibration period of the material, one can better understand the subsequent processes that follows when the surface of the material is irradiated sufficiently above the breakdown threshold. With a nanosecond laser, the pulse duration is longer than the time required for electron-phonon interaction

and thermal conduction. This permits significant absorption of laser radiation and heat transfer into the material with an increase in surface temperature. With irradiance levels of about 10^8 W/cm^2 within the nanosecond scale regime, the material is thermally vaporized though non-thermal ablation. If the irradiance is high enough, distinct phase transitions are observed from solid – liquid – vapor – plasma might coexist [18][25][26]. Because of the long pulse duration, the trailing laser pulse lasts during plasma formation and expansion; and reabsorbed by the induced plasma. The plasma is reheated and an increasing ionization degree is observed, causing what is known as plasma shielding [18].

Plasma ignition

Without preexistence of conduction electrons in the focal volume of the laser beam, it would be difficult to create a LIBS plasma. Electrons might be viewed as the receptacle of laser radiation in order to prompt laser-matter interaction from which a plasma is created. However, these conduction electrons depend on the sample material. Conductors provide free electrons already while dielectrics need a minimum energy large enough to overcome the band gap, transferring an electron from the valence band to the conduction band. In order to observe plasma ignition or breakdown, it first requires precursor electrons to then generate sufficient electron and ion densities. The absorption of photons by electrons (known as inverse Bremsstrahlung) initiates a cascade or avalanche of ionization. The main ionization processes are multi-photon ionization (simultaneous absorption of many photons by electrons to be ejected from the conduction band) and thermionic emission (absorption of laser radiation by free electrons). In real situations of LIBS, initial electrons are produced by the laser pulses and are accelerated by the electric field in the optical pulse during collision with neutral species, thus causing

9

thermalization of electrons. Electrons gather enough energy to ionize an atom or molecule, generating a cascade of electrons necessary for the formation of a plasma. Thermal processes being dominant in nanosecond ablation as laser pulse-surface interaction last, a rise of temperature at the material surface is observed, which eventually leads to melting and vaporization of the material [18][25][26][27][28].

Plasma expansion and emission

Once a plasma is formed, it evolves rapidly towards the laser source. Plasma expansion is closely linked to the details of the resulting ablation, that is, the amount of mass removed, the pressure of the environment, laser characteristics (such as the energy delivered and the beam's spot size) [27]. As the plasma cools down, it emits neutral and ionic atomic lines and possibly molecular bands. These spectral emissions depend on the intrinsic properties of the constituent atoms and the excitation conditions. Also, a broad-band continuum, resulting from electron–ion recombination and free–free interactions, is superimposed on these emission lines. Electron-ion recombination gives rise to radiative emission transitions when ions capture an electron with a transition to a bound energy state. Free-free interactions result in free-free emission transitions after loss of kinetic energy by an electron in the field of an ion. The loss of kinetic energy by an electron induces a deceleration of the electron, known as Bremsstrahlung [1][18]. In order to optimize LIBS analytical lines, spectra are temporally resolved with emission being recorded within a gate delay with minimum continuum emission. Time evolution of the LIBS signal after initial laser pulse is shown in Figure 1.2.

10
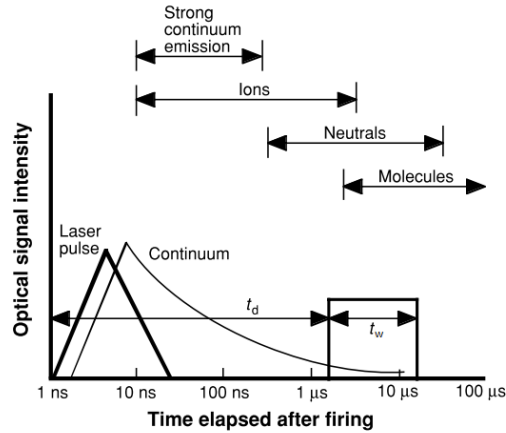
Figure 1.2   Time evolution of continuum and line radiation

Atomic, ionic and molecular emission time window. Adapted from *Laser-Induced Breakdown Spectroscopy: Fundamentals and Applications* by Miziolek [1].

Plasma characterization

Although LIBS presents great advantages, qualitative and quantitative information from collected spectra depend on plasma quality. LIBS plasmas, in which electron collision is the rate-determining mechanism, can be described by a state known as Local Thermodynamic Equilibrium (LTE). In this state, the collision processes must be much more important than the radiative ones so that the non-equilibrium of radiative energy can be neglected, while for every point within the plasma, it is still possible to find a temperature parameter that satisfies the Boltzmann, Saha and Maxwell distributions. Thus, the plasma electronic excitation temperature, T_e, and the electron density, N_e, which can be derived from the plasma emission data, can be used to describe the plasma characteristics [1]. Besides the LTE condition, the plasma should also be optically thin and stoichiometric. Stoichiometry refers to a plasma whose elemental composition is representative of the sample under study. An optically thin plasma refers to a plasma which is transparent so that radiation from the plasma volume is able to

11

escape without being reabsorbed or scattered. Emission lines from the lowest excited energy levels to the lowest energy level (the ground state) have the largest probability of being reabsorbed. These lines are called resonance lines and the phenomenon is known as self-absorption. Self-absorption is characterized by a broadened spectral profile with a flat peak. A plasma is characterized by evaluating the electron plasma temperature and electron density.

Plasma electron temperature

Depending on the experimental conditions, various methods, such as the relative intensity ratio, Doppler profile or Boltzman plot are used. However since obtaining accurate relative intensities is difficult and the Doppler effect is not the main cause of broadening in LIBS, many lines are chosen to produce a Boltzmann plot, from which the temperature is graphically obtained. The Boltzmann plot equation is used for this purpose (Equation 1.1) [1].

$$\ln\left(\frac{I_{ik}\lambda_{ik}}{g_iA_{ik}}\right) = -\frac{E_k}{k_BT} + \ln\left(\frac{n^s}{U^{s(T)}}\right) \tag{1.1}$$

where $I(a.u)$ is the line intensity, $\lambda(nm)$ is the wavelength, g_i the statistical weight of the upper energy level and $A(s^{-1})$ the transition probabilty of the atomic levels, $E(eV)$ the energy, $k_B(eV/K)$ is Boltzmann constant, $T(K)$ is the temperature, $n^s(cm^{-3})$ and U^s are, respectively, the partition function and the number density of specie s. (i corresponds to the upper energy level and k corresponds to the lower energy level). The atomic data are taken from the online NIST Atomic Spectra Database [29]. The plot of the left-hand side of (Equation 1.1) against E_k yields a slope ($-1/k_BT$), from which the temperature T is readily obtained.

12

Plasma electron number density

Stark broadening and Saha-Boltzmann methods are used for measuring the electron number density N_e [1]:

$$\Delta\lambda_{Stark} = 2w\left(\frac{N_e}{10^{16}}\right) \tag{1.2}$$

where $\Delta\lambda_{stark}(nm)$ is the full-width-at-half-maximum (FWHM), w is temperature dependent and represents the electron impact parameter, often referenced from Griem [30].

$$N_e = \frac{2(2\pi m_e k_B T)^{\frac{3}{2}}}{h^3}\frac{I_{mn}^I A_{ik}g_i^{II}}{I_{ik}^I A_{mn}g_m^I}e^{\frac{E_{ion}+E_i^{II}-E_k^I}{k_B T}} \tag{1.3}$$

where $m_e(kg)$ and $h(eV.s)$ are the mass of electron and Planck's constant, respectively; mn, ik, A_{ik}, A_{mn}, g_i, g_m, E_i, E_k, k_B and T are defined as before. (m and i correspond to the upper level while n and k correspond to the lower level.) E_{ion}, indicates the ionization energy, I and II are different ionization states. Typical electron densities of laser-induced plasmas range from 10^{16} to 10^{19} cm^{-3} [1].

Principle of laser-induced breakdown spectroscopy

Plasma is produced by the interaction of the laser pulse and the sample (liquid, solid or gas). As the plasma decays, it emits specific radiation for each element contained in the plasma which is assumed to be stoichiometric (that is having the same composition as the sample). This emission is then spectrally and temporally resolved and detected by means of a spectrometer associated with an ICCD camera. Laser-induced breakdown spectroscopy relies on the analysis of spectra obtained from well characterized plasmas. By measuring the line intensities and wavelength of the emitted species, one can analyze the data and obtain qualitative results (uniquely characterize corresponding atoms, ions, and molecules; subsequently asserting their presence in the plasma) and quantitative

13

results (how much of an element do we have in the sample). This is in summary, the principle of LIBS as outlined in Figure 1.3.
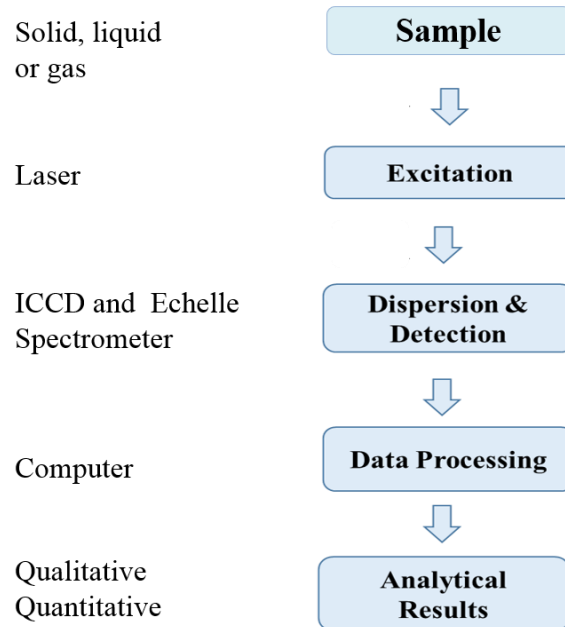
Figure 1.3   Principle of laser-induced breakdown spectroscopy

Advantages of laser-induced breakdown spectroscopy.

Compared with other chemical analysis techniques, the laser-induced technique is advantageous because of:

- Its relatively fast response time, real-time capability with results available instantly.

- Minimum sample preparation.

- Experimentally simple setup and adaptability to a variety of different measurement scenarios.

- Ability to sample gases, liquids, and solids.

- Good sensitivity for some elements (e.g., Cl, F, C) that are difficult to monitor with conventional AES methods.

14

- Using only optical emission, it allows remote sensing and *in situ* analysis useful in hazardous and otherwise inaccessible situations.

- Limits of reproducibility due to variation in laser spark and resultant plasma.

Despite these advantages, the figures of merit of laser-induced breakdown spectroscopy are constantly being improved to compete with traditional chemical analysis techniques.

Factors affecting analytical capability of laser-induced breakdown spectroscopy.

Even though the detection limit is typically in the parts-per-million (ppm) range, LIBS' main drawbacks are its precision and accuracy. These drawbacks are the direct consequences of the very advantages of the technique. For analytical purposes, it is assumed that the LIBS plasma is optically thin, in local thermodynamic equilibrium, and, most importantly, stoichiometric. In effect the stoichiometric conditions of LIBS, suggests that the elemental composition of the plasma is representative of the elements in the original sample under investigation.

Sample preparation and sample environment

The little or no sample preparation affects the homogeneity of the sample; because laser ablation only removes a few ng of the original sample, the ablated mass might not be homogeneous and the accuracy is affected. To improve the homogeneity, we rotate the sample on a platform so that each laser pulse hits a fresh spot. Accuracy and precision are improved by recording multiple spectra and averaging them. Regarding the sample environments, elements not part of the sample may contaminate the plasma. These contaminants might be from the surrounding gases, like oxygen or nitrogen, or the

15

carbon ensued from the ablation in air. However, these lines can be discarded by through spectral line selection based on prior knowledge of the sample. If a strong line of one element is observed, other lines of the same element should also be present. If multiple lines of this element are not found, this spectral line is considered not to be from the initial sample. Prior to recording the analytical spectra, background measurements are first taken and later subtracted from the sample measurements. This helps remove lines which do not originate from the investigated sample.

Laser energy and background continuum.

Fluctuations of the laser energy also affect the reproducibility of LIBS plasmas and hence the emission intensity that varies from one laser pulse to another. The fast decay of the plasma also requires that emission is recorded before the plasma completely cools down while avoiding the continuum. This is often achieved by using gated devices, like intensified charge coupled device (ICCD) detectors, to select an appropriate gate delay (t_d) and gate width (t_w). Gate delay is the time delay between plasma formation and the recording of the plasma emission. Gate width is the time over which the plasma emission is recorded. The gate delay is optimized by plotting the signal-to-noise ratio (SNR) and the signal-to-background ratio (SBR) against time. Thus, with appropriate experimental conditions, most of these drawbacks can be substantially reduced.

Qualitative analysis

Qualitative analysis consists of identifying the presence of a given element in a sample from the recorded spectra. To do this, one might consider various parameters like:

- Knowledge of the sample. This helps eliminate other spectral lines unless the sample is contaminated.

16

- Relative intensities of the lines from reference tables like the NIST atomic database which are then compared the LIBS spectra.

- The ionization stage of the element. Neutral species are preferred over doubly or triply ionized species when these lines interfere.

- Multiple strong lines of the same element. If one strong line of one element is observed, others should also be present.

Quantitative analysis

Quantitative analysis relies on calibration curves. These curves are used to relate the amount of analyte (concentration or mass) to the measured response (intensity). In order improve the precision and accuracy of LIBS, emission lines used should be carefully selected such that they are not affected by spectral interference and self-absorption.

Univariate calibration is commonly used as a standard approach to obtain quantitative information, like concentration and limit of detection (LOD), from LIBS spectra. LIBS analysis assumes the plasma to be optically thin and stoichiometric. With these assumptions, one can write the spectral line intensity I_{ij} as follows

$$I_{ij}=FC^s \qquad\qquad (1.3)$$

where F is the experimental factor and C^s the analyte concentration. However, it is difficult to handle shot-to-shot variations of the laser pulse and matrix effects (influence of physical and chemical properties of sample on the emission lines) associated with LIBS by this method, even though an internal standard has been used to reduce these effects to some extent [1] [27]. Multivariate approaches which are well established for inductively coupled plasma−optical emission spectrometry (−mass spectrometry) (ICP-OES or ICP-MS) [31][32][33][34][35], have been applied to LIBS with satisfactory results, using partial least squares (PLS), principal component analysis

17

(PCA), and multiple linear regression (MLR). PLS has been used to analyze precious metals and to quantify major elements in heterogeneous and homogeneous samples from time-unresolved spectra [36][37]. Elemental analysis of igneous rock powders has been demonstrated for prediction of major element compositions [38]. Ayyalasomayajula *et al.* used three calibration approaches (univariate calibration, MLR and PLS) for the study of slurry; the results with PLS corroborated those of ICP-OES [39]. Stipe *et al.* compared univariate and PLS for steel samples, based on their standard and relative error of prediction (SEP) and (REP), respectively. Predictions made with a calibration model using iron as an internal standard resulted in the lowest REP. They found that for manganese and chromium, PLS performed as well as the internal standard method. They reported that the REP for all elements may be improved by optimizing experimental parameters, such as lens-to-sample distance, laser pulse energy, and spectrometer delay and gate times, which they held constant in their study [40].

- Principal component analysis (PCA) seeks the hidden structure within a large set of complex data, such as spectroscopic data. The input to the PCA calibration method is the peak information obtained from analysis of the spectral data. The most significant information carried by the original variables are projected onto a smaller number of latent variables called principal components (PC). From these projections, the loading plots and score plots provide information on the relative contribution of the various spectral lines being used.

- Partial least squares regression (PLS-R) provides a calibration model for the relationship between a set of predictor variables X (spectra) and a set of response variables Y (concentration). If the spectral data contain information about the properties (concentration) of interest, a reliable calibration model can be constructed. The samples with known elemental concentrations are used to create a model relating Y to X that is used to predict the concentrations of unknown specimens.

18

Analytical figures of merit of LIBS

For laser-induced breakdown spectroscopy, like other analytical chemistry techniques, its analytical capabilities are evaluated from its figures of merit. Amongst these are the limit of detection (LOD), precision and accuracy which are commonly used [27]. Limit of detection (LOD) is defined as the smallest concentration of an analyte that can reliably be detected given an analytical technique [41].

$$\begin{cases} LOD = 3\frac{c\sigma_s}{I} \\ LOD = 3\frac{\sigma_s}{S} \end{cases} \tag{1.4}$$

- where c, I, and σ_s are the concentration, intensity, and standard deviation of the blank measurement of the lowest concentration, respectively. S is the slope of the univariate calibration curve.

- Precision describes the measurement repeatability which is often affected by the shot-to-shot instabilities of laser pulse, which perturb the plasma. This repeatability is also affected by the homogeneity of the sample.

$$s_d = \left[\sum \frac{(x_i - M)^2}{n-1}\right]^{1/2} \tag{1.5}$$

- where s_d, x_i, M and n are the standard deviation, value of ith measurement, averaged measurement and the total number of measurement, respectively.

- The percent accuracy error %RA is used to measured how close a measurement (C_{LIBS}) is to the reference value of the concentration (C_{ref}). This reference value is given by certified samples or standard techniques like ICP or mass spectrometry.

$$\%RA = \frac{|C_{LIBS} - C_{ref}|}{C_{ref}} \tag{1.6}$$

Research motivation and objective

Quite often in elemental analysis, the sample under investigation does not contain only a single element. Rather it is made of several elements. It then becomes onerous, expensive and above all time consuming to proceed with the analysis one element at a

19

time when fast response is required. A multi-elemental approach would therefore be the best option. Laser-induced breakdown spectroscopy by its simplicity, little to no sample preparation, and broad wavelength (ultraviolet to visible) coverage can record within a single spectrum, almost all elements in the periodic tables in a very short time. Hence, offering a possibility of simultaneous multi-elemental analysis with results than can be available in real time, and by this, reduce the analytical time. Also, in certain cases, the samples are found in harsh or difficult to reach environments, such as geological samples. As such, *in situ* analysis becomes almost impossible with conventional analytical chemistry techniques. However, the optical emission nature of LIBS makes it suitable for remote sensing and analysis in such environments. Laser-induced breakdown spectroscopy was then used for simultaneous multi-elemental analysis and geological applications. The objectives of this dissertation were to:

1. Use LIBS as a tool for multi-elemental analysis and develop a screening and classification pattern for pharmaceutical products.

2. Analytically reduce matrix effect in matrices with varying concentrations through a case study of slags.

3. Use LIBS for elemental characterization of geological samples through a case study of shales.

4. perform LIBS studies for elemental analysis with application to underwater carbon sequestration.

   To achieve these objectives, several samples were used, notably solids and liquids. The solids employed were in powder form. Univariate and multivariate analyses

were used for qualitative, and quantitative analysis and results compared with those of standard techniques, namely inductively coupled plasma-optical emission spectroscopy.

Dissertation structure

This dissertation focuses on applications of laser-induced breakdown spectroscopy to pharmaceutical products, slags, and geological samples. The chapters hereinafter (except Chapter 2 which is under peer-review process to appear in *Spectrochemica Acta Part B: Atomic Spectroscopy* journal and chapter 5 which is in preparation to be submitted to the same journal) are peer-reviewed published journal articles. For this reason, they are structured as self-contained entities.

Chapter 2: Feasibility of rapid multi-elemental analysis and screening of cosmetic powders based on the raw material used is investigated in chapter 2. Most cosmetic powders are essentially made from talc because of its softness. However, the potential presence of asbestos in talc is of concern in pharmaceutical products and their cosmetic usage. The similarity in the chemical structure of talc and asbestos coupled to the fact that they occur in the nature together have raised concern about asbestos-free talcum cosmetics. An alternative raw material (amongst which is starch) is now considered.

Chapter 3: A byproduct of coal gasification is characterized by analyzing its elemental composition. An inductively coupled plasma is often used for this purpose. We propose the use of LIBS for its simplicity and capability of real time analysis. Chapter 3 has been published in *Spectrochemica Acta Part B: Atomic Spectroscopy.*

Chapter 4: In this chapter, we are interested in the determination of elemental composition of geological samples using laser-induced breakdown spectroscopy. The case study of Marcellus shales is investigated for its potential use in the carbon

sequestration process. This chapter has been published in *Spectrochemica Acta Part B: Atomic Spectroscopy.*

Chapter 5: Optical emission of underwater plasma with application to carbon sequestration is performed in this chapter. The effects of high pressure on the plasma and the quantitative analysis of trace elements is studied.

Chapter 6: Research summary and recommendations on future work are presented.

References

[1]   A. Miziolek, V. Palleschi, and I. Schechter, *Laser Induced Breakdown Spectroscopy: Fundamentals and Applications*. Cambridge University Press, 2006.

[2]   G. L. Moore, *Introduction to Inductively Coupled Plasma Atomic Emission Spectrometry*. Elsevier, 2012.

[3]   L. Radziemski, "From LASER to LIBS, the path of technology development," *Spectrochim. Acta Part B At. Spectrosc.*, vol. 57, pp. 1109–1113, 2002.

[4]   T. R. Loree and L. J. Radziemski, "Laser-induced breakdown spectroscopy: Time-integrated applications," *Plasma Chem. Plasma Process.*, vol. 1, pp. 271–279, 1981.

[5]   G. C. Dacey, "Optical masers in science and technology," *Science)*., vol. 135, no. 3498, pp. 71–74, 1962.

[6]   M. Baudelet and B. W. Smith, "The first years of laser-induced breakdown spectroscopy," *J. Anal. At. Spectrom.*, vol. 28, p. 624, 2013.

[7]   J. D. Winefordner, I. B. Gornushkin, T. Correll, E. Gibb, B. W. Smith, and N. Omenetto, "Comparing several atomic spectrometric methods to the super stars: special emphasis on laser induced breakdown spectrometry, LIBS, a future super star," *Journal of Analytical Atomic Spectrometry*, vol. 19. p. 1061, 2004.

[8]   F. Brech and L. Cross, "Optical microemission stimulated by a ruby maser," *Appl. Spectrosc*, vol. 16, p. 59, 1962.

[9]   J Debras-Guédon and N. Liodec, "De l'utilisation du faisceau d'un amplificateur a ondes lumineuses par émission induite de rayonnement (laser á rubis), comme source énergétique pour l'excitation des spectres d'émission des éléments," *CR Acad Sci*, vol. 257, pp. 3336–39, 1963.

[10]   J. Debras-Guédon and N. Liodec, "Sur une extension des possibilités de l'analyse spectrale dans le domaine del'analyse ponctuelle par utilisation d'un laser," *Bull. Soc. Fr. Ceram.*, pp. 61–68, 1963.

[11]   D. G. and F. B. R. C. Rosan, "Progress in laser microprobe emission spectroscopy," *Fed. Proc.*, vol. 24, p. 542, 1964.

[12]   E. F. Runge, R.W. Minck, and F.R. Bryan, "Spectrochemical analysis using a pulsed laser," *Spectrochimica Acta Part B: Atomic Spectroscopy*, vol. 20. pp. 733–35, 1964.

[13]   H. M.-B. Moenke, *Laser Micro- Spectrochemical Analysis*. Crane, Russak & Co, New York, 1973.

[14]   S. Maurice, R. C. Wiens, M. Saccoccio, B. Barraclough, O. Gasnault, O. Forni, N. Mangold, D. Baratoux, S. Bender, G. Berger, J. Bernardin, M. Berthé, N. Bridges, D. Blaney, M. Bouyé, P. Caïs, B. Clark, S. Clegg, a. Cousin, D. Cremers, a. Cros, L. Deflores, C. Derycke, B. Dingler, G. Dromart, B. Dubois, M. Dupieux, E. Durand, L. D'Uston, C. Fabre, B. Faure, a. Gaboriaud, T. Gharsa, K. Herkenhoff, E. Kan, L. Kirkland, D. Kouach, J. L. Lacour, Y. Langevin, J. Lasue, S. Le Mouélic, M. Lescure, E. Lewin, D. Limonadi, G. Manhès, P. Mauchien, C. McKay, P. Y. Meslin, Y. Michel, E. Miller, H. E. Newsom, G. Orttner, a. Paillet, L. Parès, Y. Parot, R. Pérez, P. Pinet, F. Poitrasson, B. Quertier, B. Sallé, C. Sotin, V. Sautter, H. Séran, J. J. Simmonds, J. B. Sirven, R. Stiglich, N. Striebig, J. J. Thocaven, M. J. Toplis, and D. Vaniman, "The ChemCam instrument suite on the Mars Science Laboratory (MSL) rover: Science objectives and mast unit description," *Space Sci. Rev.*, vol. 170, pp. 95–166, 2012.

[15]   H.D.Mott-Smith, "History of Plasma," *Nature*, vol. 233. p. 219, 1971.

[16]   R. Noll, *Laser-induced breakdown spectroscopy, fundamentals and applications*. Springer Berlin Heidelberg, 2012.

[17]   R. E. Russo, "Laser Ablation," *Appl. Spectrosc.*, vol. 49, no. 9, p. 14A–28A, 1995.

[18]   J. P. Singh and S. N. Thakur, *Laser-induced breakdown spectroscopy*. Elsevier, 2007.

[19]   G. S. Senesi, "Laser-induced breakdown spectroscopy (LIBS) applied to terrestrial and extraterrestrial analogue geomaterials with emphasis to minerals and rocks," *Earth Sci. Rev.*, vol. 139, pp. 231–267, 2014.

[20]   K. L. Eland, D. N. Stratis, D. M. Gold, S. R. Goode, and S. M. Angel, "Energy dependence of emission intensity and temperature in a LIBS plasma using femtosecond excitation," *Appl. Spectrosc.*, vol. 55, no. 3, pp. 286–291, 2001.

[21]   K. L. Eland, D. N. Stratis, T. Lai, M. a. Berg, S. R. Goode, and S. M. Angel, "Some comparisons of LIBS measurements using nanosecond and picosecond laser pulses," *Appl. Spectrosc.*, vol. 55, no. 3, pp. 279–285, 2001.

[22]   R. E. Russo, X. L. Mao, C. Liu, and J. Gonzalez, "Laser assisted plasma spectrochemistry: laser ablation," *J. Anal. At. Spectrom.*, vol. 19, no. 9, p. 1084, 2004.

[23]   A. Semerok, C. Chaléard, V. Detalle, J.-L. Lacour, P. Mauchien, P. Meynadier, C. Nouvellon, B. Sallé, P. Palianov, M. Perdrix, and G. Petite, "Experimental investigations of laser ablation efficiency of pure metals with femto, pico and nanosecond pulses," *Appl. Surf. Sci.*, vol. 138–139, pp. 311–314, 1999.

[24]   X. Zeng, X. L. Mao, R. Greif, and R. E. Russo, "Experimental investigation of ablation efficiency and plasma expansion during femtosecond and nanosecond laser ablation of silicon," *Appl. Phys. A Mater. Sci. Process.*, vol. 80, pp. 237–241, 2005.

[25]   A. De Giacomo, M. D. Aglio, R. Gaudiuso, S. Amoruso, and O. De Pascale, "Effects of the background environment on formation , evolution and emission spectra of laser-induced plasmas," *Spectrochim. Acta Part B At. Spectrosc.*, vol. 78, pp. 1–19, 2012.

[26]   C. Boulmer-Leborgne, J. Hermann, and B. Dubreuil, "Plasma formation resulting from the interaction of a laser beam with a solid metal target in an ambient gas," *Plasma Sources Sci. Technol.*, vol. 2, no. 3, pp. 219–226, 1993.

[27]   D. Cremers and L. Radziemski, *Handbook of Laser–Induced Breakdown Spectroscopy,* 2nd ed., John Wiley & Sons, 2013.

[28]   A. Bogaerts, Z. Chen, R. Gijbels, and A. Vertes, "Laser ablation for analytical sampling : what can we learn from modeling ?," *Spectrochim. Acta Part B At. Spectrosc.*, vol. 58, pp. 1867–1893, 2003.

[29]   "http://physics.nist.gov/PhysRefData/ASD/lines_form.html." .

[30]   H. Griem, *Spectral line broadening by plasmas*. Academic Press, New York, 1974.

[31]   M. Grotti, "Improving the analytical performances of inductively coupled plasma optical emission spectrometry by multivariate analysis techniques.," *Ann. Chim.*, vol. 94, no. 1–2, pp. 1–15, Jan. .

[32]   M. Glick, K.R. Brushwyler, and G.M. Hieftje, "Multivariate calibration of a photodiode array spectrometer for atomic emission spectroscopy," *Appl. Spectrosc.*, vol. 45, no. 3, pp. 328-333, 1991.

[33]   J. C. Ivaldi, D. Tracy, T. W. Barnard, and W. Slavin, "Multivariate methods for interpretation of emission spectra from the inductively coupled plasma," *Spectrochim. Acta Part B At. Spectrosc.*, vol. 47, no. 12, pp. 1361–1371, Nov. 1992.

[34]   G. K. and K.-H. B. K. Venth, K. Danzer, "Multi Signal evaluation in ICP MS, determination of trace elements in molybdenum zirconium alloys," *Fresenius J. Anal. Chem*, vol. 354, no. (7-8), pp. 811–817, 1996.

[35]   M. Rupprecht and T. Probst, "Development of a method for the systematic use of bilinear multivariate calibration methods for the correction of interferences in inductively coupled plasma-mass," *Anal. Chim. Acta*, vol. 358, no. 3, pp. 205-225, 1998.

[36]   J. Amador-Hernández, L.E. Garcia-Ayuso, J.M. Fernández-Romero, and M.D. Luque de Castro,"Partial least squares regression for problem solving in precious metal analysis by laser induced breakdown spectrometry," *J. Anal. At. Spectrom.,* vol. 15, no. 6, pp. 587–593, Jan. 2000.

[37]   J. . Luque-García, R. Soto-Ayala, and M.D. Luque de Castro, "Determination of the major elements in homogeneous and heterogeneous samples by tandem laser-induced breakdown spectroscopy–partial least square regression," *Microchem. J.*, vol. 73, no. 3, pp. 355–362, Dec. 2002.

[38]   J. M. Tucker, M. D. Dyar, M. W. Schaefer, S. M. Clegg, and R. C. Wiens, "Optimization of laser-induced breakdown spectroscopy for rapid geochemical analysis," *Chem. Geol.*, vol. 277, no. 1–2, pp. 137–148, Oct. 2010.

[39]   K. Ayyalasomayajula, V. Dikshit, F.Y. Yueh, J.P. Singh, and L.T. Smith, "Quantitative analysis of slurry sample by laser-induced breakdown spectroscopy," *Anal. Bioanal. Chem.*, vol. 400, no. 10, pp. 3315–3322, 2011.

[40]   C. B. Stipe, B. D. Hensley, J. L. Boersema, and S. G. Buckley, "Laser-induced breakdown spectroscopy of steel: a comparison of univariate and multivariate calibration methods," *Appl. Spectrosc.*, vol. 64, no. 2, pp. 154–60, Mar. 2010.

[41]   A. D. McNaught and A. Wilkinson, *Compendium of Chemical Terminology*, vol. 1669. Oxford: Blackwell Science, 1997.

CHAPTER II

MULTIVARIATE APPROACH FOR QUALITATIVE ANALYSIS IN LASER-
INDUCED BREAKDOWN SPECTROSCOPY CASE OF COSMETIC
TALCUM POWDER[1]

Abstract

In the present study, laser-induced breakdown spectroscopy was applied to talc-
and starch-based baby powders for elemental analysis, screening and classification based
on the raw material used. Major elements, such as Si, Fe and Mg, were qualitatively
identified as well as minor elements, such as Ca, Na and K. CN molecular bands were
identified in the starch sample. With the aid of principal component analysis (PCA) and
internal standardization, talc-based cosmetic powder could be differentiated from starch-
based. Principal component analysis further showed that Mg was the main element
responsible for the grouping of the samples into starch- versus talc-based. The PCA
results also attributed the subgrouping within the talc-based powder to Ca. The
combination of internal standardization with Si as internal standard and principal
component analysis approaches showed that LIBS can be used for rapid elemental
analysis and classification of cosmetic powders. The low intensity ratios of Mg/Si and

---

[1] Most of the content in this chapter is adapted from a paper to be submitted authored by Hervé K. Sanghapi
with participation of Bader Alfarraj, Charles Ghany, Krishna K. Ayyalasomayajula, Fang Y.Yueh, Jagdish
P. Singh, A. Farooq and A. Muhammad.

Fe/Si observed in talcum powder show that these two ratios could be used as indicators of the potential presence of asbestos.

Introduction

Most cosmetic powders are essentially made from talc because of its softness. However, the potential presence of asbestos in talc is of concern for human health and in pharmaceutical products [1] [2]. Talc is a hydrated magnesium silicate with chemical formula $Mg_3Si_4O_{10}(OH)_2$ which is similar to that of asbestos, a naturally occurring hydrated silicate. The similarity in the chemical structure of talc and asbestos coupled with the fact that they occur in the nature together have raised concerns about asbestos-free talcum cosmetics [3]. The production and use of asbestos-containing products are regulated and in some countries, like Japan, a content of more than 1% is prohibited [4]. According to several authors, perennial application of talcum-based products is susceptible of causing endometrial and ovarian cancers, based on its similarity to asbestos [5][6][7][8]. Nowadays alternative sources, like cornstarch, are found on the market in replacement of talcum. Whysner and Mohan [9] assessed the ovarian cancer risk for perineal application of starch and talc. In comparing the chemical natures of the two powders, he observed that whereas associations between talc exposure and ovarian cancer could suggest causal relationship, the application of powder containing cornstarch exclusively is not predicted to be a risk factor for ovarian cancer. There is a need for careful chemical analysis by manufacturers to make sure that talc used in cosmetics is asbestos free.

Analytical techniques, such as transmission electron microscopy (TEM), scanning electron microscopy equipped with energy dispersive X-ray spectroscopy (SEM–EDS),

28

and polarized light microscopy (PLM), have been used to investigate the presence asbestos. Light scattering and Raman spectroscopy have also been used [10][11][12]. Gordon *et al*. [13] reported the presence of asbestos in cosmetic talcum powder as a cause of mesothelioma in women; they used TEM in conjunction with EDS and selected-area electron diffraction (SAED) to determine asbestos fiber number and type. However, these techniques are cumbersome, time consuming and require significant hands-on experience. Sometimes these techniques are suitable only for elements with atomic number $Z > 28$. The low concentration and small dimensions of asbestos fibers also make their characterization difficult [14]. Consequently, there is a need for simplified, fast and sensitive technique capable of analyzing all elements and laser-induced breakdown spectroscopy is such a technique with detection limits on the order of ppm. LIBS has been proposed to characterize various types of asbestos (Chrysotile, Crocidolite, Amosite, Anthophyllite, Actinolite, and Tremolite). The intensity ratios of Mg/Si and Fe/Si were used as intrinsic characteristic of asbestos [15] [16]. Caneve *et al*. [15] reported a correlation between the intensity ratios (Mg/Si and Fe/Si) of LIBS and the concentration ratios (Mg/Si and Fe/Si) from energy dispersive X-ray spectroscopy (EDS). A good linear regression fit was used to confirm the proportionality between the ratios of intensity and concentration for the chosen pairs of elements.

Laser-induced breakdown spectroscopy (LIBS) is a robust analytical technique with greater prospects as presented by Winefordner *et al*. [17] and several textbooks on LIBS have been published on this technique [18][19][20] [21]. LIBS consists of generating a plasma by focusing a laser pulse on the sample. The optical emission from the plasma collected by a spectrometer, is used for qualitative analysis (identification of

29

elements) and for quantitative analysis (sample composition through calibration curves). Temporally and spatially resolved plasmas provide great advantages over other standard analytical techniques. Without being exhaustive, amongst others advantages, are LIBS's ability for *in situ* and stand-off analysis due to the use of fiber optics, multi-elemental analysis at low and high atomic number, real time and fast analysis, and little sample preparation [21]. These features have made LIBS a workhorse in many disciplines (material science, forensic science, biological science and chemical and pharmaceutical industries) and used extensively on solids, liquids and aerosols [20][22].

Despite the versatility of LIBS, its application to direct analysis of powder samples has been a major challenge due to the amount of sample that gets and subsequent scattering during radiation by laser pulses. To overcome such an undesirable effect, pellets have been used [23][24][25][26]. The sample is mixed with a binder, such as polyvinyl alcohol (PVA), and then pressed into pellets. This technique is limited by the procedure cost and sometimes the sample available is too small to make a pellet. Alternative methods of LIBS operating under low-pressure ambient gas have been reported with spectrochemical analysis being performed directly on powder samples with the disadvantage that it might be denatured in the process [27][28][29]. A thin film using an ultraviolet Nd:YAG laser at 355 nm has also been used, but films may suffer from inhomogeneity [30]. In this work, we used a simple and low-cost sampling method. It consists of sticking a double-sided tape on a laboratory glass slide and uniformly distribute a small amount of sample on the other side of the tape. Elemental analysis of cosmetic powder is herein reported using LIBS.

30

The figure of merit of LIBS relies on the quality of the emission lines obtained from the plasma. Although capable of multi-elemental analysis, spectral interference with LIBS is common and affects the peak identification and calibration curves. However, plasmas can be temporally and spatially resolved in order to mitigate this. Data processing techniques have also been developed to minimize spectral interference and background reduction in order to improve quantitative analysis of LIBS [31][32][33]. Amongst these multivariate analysis has been used to improve the quantitative results of LIBS, notably by applying partial least squares regression (PLSR), principal component analysis (PCA) or multiple linear regression (MLR) [34][35][36][37][38]. Principal component analysis, which is a more qualitative approach, is used principally for classification [34][39][40]. Principal component analysis seeks the hidden structure within a large set of complex data such as spectroscopic data.

In the present study, we qualitatively investigated cosmetic powder using laser-induced breakdown spectroscopy. Intensity ratio and multivariate principal component analysis are used to screen and classify some cosmetic powders found on the market based on the raw material used for their manufacturing. Prior to the qualitative analysis of this study, the plasma is characterized by evaluating its electron number density and the electron temperature. PCA is performed using Unscrambler X version 10.3 software from CAMO Software AS, Oslo Science Park, Norway.

Experimental

Apparatus

The apparatus used for our experiment is shown in Figure 2.1.
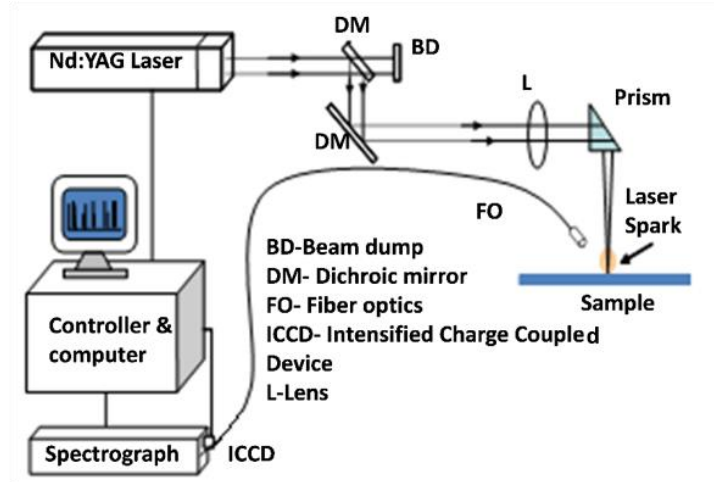
Figure 2.1   LIBS experimental setup for cosmetic powder analysis.

A frequency-doubled Q-switched Nd:YAG laser (Quantel CFR400 20 Hz, 7-ns pulse width, 6-mm diameter, 235 mJ maximum pulse energy) was used as an excitation source. The 532-nm laser light was focused onto the sample surface using a 30-cm focal length quartz lens and a right-angle prism. The laser energy used in this study was 46 mJ. The emission from the laser-induced plasma was collected using a pick-up lens (Ocean Optics Inc. (OOI) Part No.74-UV) aligned at 45^0 with respect to the laser beam. The distance of the pickup lens from the sample was about 5 cm. The collected signal was coupled into an Andor Technology broadband spectrometer (Mechelle ME5000, 200–975 nm spectral range) through a 100-µm diameter optical fiber. The spectrograph signal was integrated with a 1024x1024 intensified charge-coupled device (ICCD) detector. The gate delay and gate width were controlled with the built-in digital delay generator (DDG) of

32

the spectrograph. The DDG is activated by the trigger pulse from the laser Q-switch output to synchronize data acquisition with the laser pulse. The spectrograph was connected to a personal computer for data acquisition. Each spectrum collected was an average of 50 laser shots to obtain a better signal-to-noise ratio. Measurements were done by uniformly putting few mg of sample on a double-sided tape already fixed on a laboratory glass slide. This was then placed on a rotating platform to ensure that fresh sample was available to interact with the laser beam. The gate width was set to 5 μs and the gate delay was varied from 0.5 to 7 μs.

Sample preparation

Five different cosmetic powders were used for this experiment and labelled as follows (P1, P2, P3, P4, and P5). Samples P1, P2, P3 and P5 are talc-based whereas P4 is mainly made of cornstarch. Talcum powder is primarily composed of magnesium silicate, it may contain variable amounts of associated minerals, such as calcite (calcium carbonate) and dolomite(calcium and magnesium carbonate) [2]. Small amounts of sample were scattered on a double-sided tape already fixed on a laboratory glass slide. Reported spectra are averaged over five spectra with each being an accumulation of fifty laser shots. In this chapter, talc-based and cornstarch-based cosmetics will be referred to as "talcum" and "starch", respectively.

Results and discussion

Plasma characterization

In order to retrieve qualitative and quantitative information from collected spectra, plasmas should satisfy certain conditions. Principally, it should be optically thin,

33

in local thermodynamic equilibrium (LTE), and stoichiometric [21]. Plasma parameters, such as the temperature and electron number density, are reported below.

Temporal gating

Time resolution in LIBS is an important factor to be considered. For example, Radziemski and Loree [42] reported its effect on the improvement of the detection limit of phosphorus and chlorine. In effect, since a plasma has a strong continuum in its early stages and its lifetime is very short (microseconds), spectral emission collection should occur after a delay during which the continuum drops and only emission lines are dominant, before it quenches. This optimum time window is obtained by evaluating the signal-to-noise ratio (SNR). The gate delay at which the maximum SNR occurs is used as the experimental gate delay. The plot of the SNR versus gate delay exhibits a certain shape as illustrated in Figure 2.2. The reported SNR is evaluated using the Ca(II) 315.88-nm line. At early gate delays, a low SNR is observed due to the strong continuum. As the plasma is cooling down and the gate delay is increased, the SNR also increases up to a certain maximum, after which it starts to drop again and even decreases below the initial value. This drop is due to the fact that the plasma cools and quenches after a short while. From Figure 2.2, our gate delay was thus optimized and all analyses were then carried with spectra collected at gate delay $t_d = 2$ μs.

34
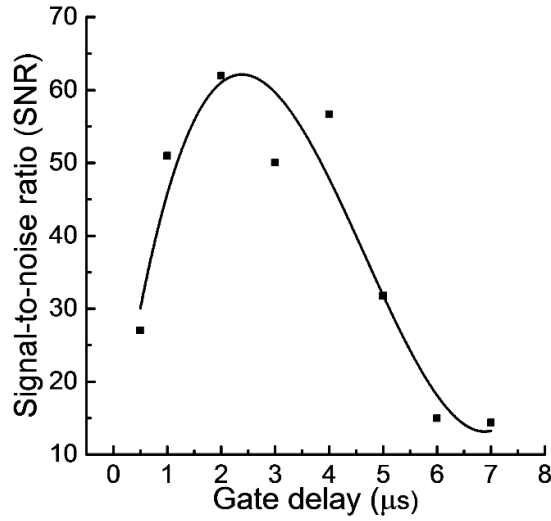
Figure 2.2   Variation of SNR versus gate delay.

Plasma temperature and electron density

For an optically thin LIBS plasma, temperature can be derived from a Boltzmann plot, using the following equation with atomic data [43] given in Table 2.1.

$$ln\left(\frac{I_{ki,Z}\lambda_{ki,Z}}{g_{k,Z}A_{ki,Z}}\right) = -\frac{E_{k,z}}{k_B T} + ln\left(\frac{Fn_Z}{P_Z}\right) \tag{2.1}$$

where *I, λ, g* and *A* are the line intensity, wavelength, statistical weight the upper level, and transition probability, respectively. *E, T, F, n* and *P* represent the excitation energy, temperature, the experimental parameter, the number density, and the partition function, respectively. Here, *k* and *i* are the electronic transition levels while *Z* represents the ionization state of the species. k_B is Boltzmann constant, defined in Table 2.1.

35

Table 2.1 Atomic data for temperature and electron number density[43]

	Wavelength (nm)	Energy (eV)	$A_{ki}g_k$ (10^8s^{-1})	g_k	Boltzmann constant K_B (10^5 eV/K)
Ca(I)	422.67	2.93	6.54	3	
Ca(II)	315.88	7.05	12.0	4	
Ca(II)	317.93	7.05	22.0	6	8.61
Ca(II)	373.69	6.46	3.40	4	
Ca(II)	393.36	3.15	5.88	4	
Ca(II)	396.84	3.12	2.80	2	

A good Boltzmann plot requires accurate line intensities and well-spaced upper levels. Reported plasma electron number density (N_e) was derived from the Saha-Boltzmann method, Equation 2.2. This method makes use of the ratio of two lines corresponding to different ionization states of the same element [21].

$$N_e = \frac{I'_Z}{I'_{Z+1}} 6.04 \times 10^{21}(T_{eV})^{3/2}exp\left(-E_{k,Z+1}+E_{k,Z}-X_Z\right) \qquad (2.2)$$

where $I_{Z'} = I_Z\lambda_{ki,Z}/g_{k,Z}A_{ki,Z}$, T_{eV} is temperature in eV, and X_Z is the ionization energy. Others terms remain the same as defined previously. Ca(I) 422.73-nm and Ca(II) 393.36-nm emission lines were used.
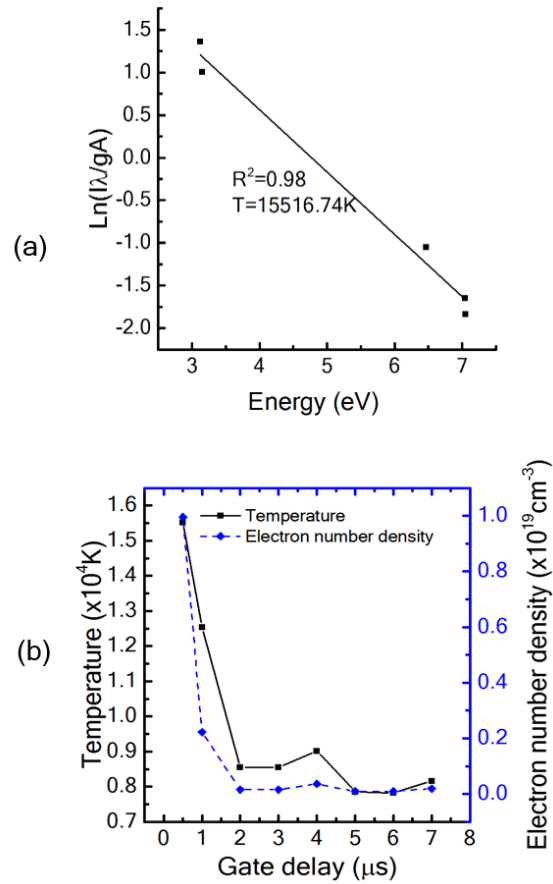
Figure 2.3   Plasma characterization

(a) Boltzmann plot, (b) Temporal evolution of electron number density and plasma temperature.

Figure 2.3 (a) shows a Boltzmann plot for temperature while Figure 2.3 (b) is the electron number density. The calculated electron number density falls within the reported literature range for LIBS: that is, 10^{16} to 10^{19} cm^{-3} [44]. A highly dense plasma is observed with a small gate delay. As the gate delay increases, the electron number density and plasma electron temperature (Figure 2.3) decrease sharply and become relatively constant after 2 μs. This can be explained by the transient nature of LIBS plasmas which vanish after a couple of microseconds.

37

Optical thinness of plasma

Radziemski *et al*. [45] used intensity ratios (Equation 2.3) as a procedural means to check the optical thinness of a plasma. Intensity ratios of resonnant and non-resonnant lines should be nearly the same as that of the statistical weights of the upper levels. The following equation was used to check this. The statistical weight are taken from the NIST atomic spectra database (Table 2.1) [43].

$$\frac{I_{ki}}{I_{nm}} = \left(\frac{\lambda_{nm,Z}}{\lambda_{ki,Z}}\right)\left(\frac{A_{ki,Z}}{A_{nm,Z}}\right)\left(\frac{g_{k,Z}}{g_{n,Z}}\right) exp\left(-\frac{E_{k,Z}-E_{n,Z}}{k_B T}\right) \qquad (2.3)$$

I$_{ki}$ and *I$_{nm}$*: the *k-i* and *n-m* transition line intensities; other terms have been previously defined. The exponential part is neglected if emission lines with close enough upper energy levels are considered. Table 2.2 summarizes the theoretical ($\lambda_{nm}g_k A_{ki}/\lambda_{ki}g_n A_{nm}$) and experimental (*I$_{ki}$/I$_{nm}$*) intensity ratios used for optical thinness.

Table 2.2 Comparison of theoretical and experimental intensity ratio for optically thin plasma at different gate delays.

Gate delay (µs)	I$_{ki}$/I$_{nm}$ (Experimental)	$\lambda_{nm}g_k A_{ki}/\lambda_{ki}g_n A_{nm}$ (Theoretical)
0.5	0.66	
1	0.61	
2	0.50	
3	0.50	
4	1.96	0.54
5	0.45	
6	0.93	
7	0.94	

The theoretical value is constant for any given pair of chosen lines because the parameters given in the equation are constant. The ratio of Ca(II) 315.88-nm/Ca(II) 317.93-nm was used. From Table 2.2, we observed that experimental ratios at 2-3 µs were close to the theoretical value. The plasma was optically thin within this gate dalay.

38

Qualitative analysis

Temporally resolved LIBS spectra of the five samples are shown in Figure 2.4.
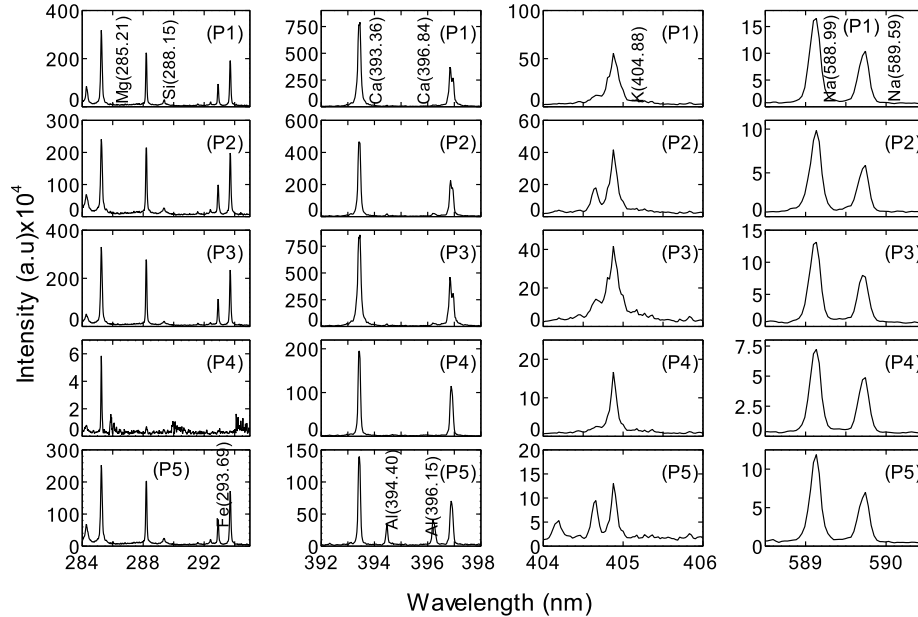
Figure 2.4   Selected emission lines from talcum (P1, P2, P3, P5) and starch (P4) baby powders.

Qualitative analysis within the chosen spectral range (284-592nm) shows the elemental composition of the samples with major and minor elements. Although magnesium lines are present in both talcum and starch samples, the strength of magnesium line is about two orders less in sample P4 (starch). Silicon and iron lines are very weak in starch. Calcium emission lines are present in all five samples with relatively different strengths. The same observation is made with sodium and potassium. Aluminum lines are observed only in sample P5. The variation in elemental composition can be explained by the nature of the raw material used. Although talcum powder is basically of magnesium silicate origin, as mentioned earlier, talcum may contain variable amounts of

39

associated minerals, such as calcite (calcium carbonate) and dolomite (calcium and magnesium carbonate). Gondal *et al*. [46] mentioned several substitutes for the main elements in talcum powder. For example, small amounts of aluminum can substitute for silicon, or Al can be substituted for magnesium or iron; and very small amounts of calcium can substitute for Mg.

Although molecular bands are observed at longer gate delays, it was possible to have both atomic and molecular emission within short gate delay which in this was optimized at 2 μs. Figure 2.5 shows the molecular bands of CN within wavelength of 386-389nm. This emission band has also been reported for short gate delay by Qianli [47]. This was observed only in the starch-based powder sample.
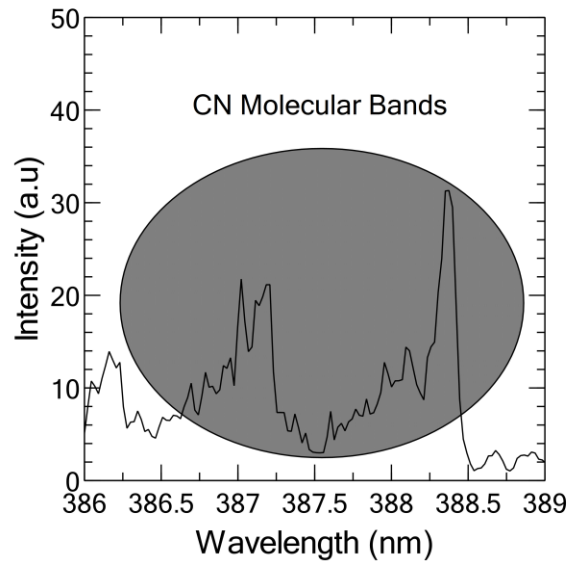
Figure 2.5   Molecular bands of CN in starch-based powder sample.

The formation of CN occurs through the following equation $C_2 + N_2 \rightarrow 2CN$, where N comes from the atmosphere. Since, under same experimental conditions, the emission band was only observed in the starch-based, we can conclude that the C originated from the starch-based sample P4. Thus, the starch nature of sample P4 is asserted by the presence of the CN molecular bands.

The spectra of the samples presented in this study highlights the possibility of using LIBS to perform direct qualitative elemental analysis of raw materials used in baby powders.

Screening of talc- and starch-based baby powders using an internal standardization

In an optically thin plasma, the relative abundance of an element can be inferred from the strength of the emission lines, assuming a linear correlation between the elemental concentration and background subtracted intensity [21]. Variation in the plasma performance due to the presence of non-analyte elements whose concentration may be constant or may be variable leads to what is known as "matrix effects", which together with the laser pulse shot-to-shot variability , increase the fluctuation of emission lines [48]. To handle this kind of problem, internal standardization and multivariate analysis are often used [48][49][50][51]. Several intensity ratios were carried out and only that with Si yielded a difference in the various samples. The intensity ratios of Na, Ca, Mg, Fe and K with respect to Si are reported in Figure 2.6.
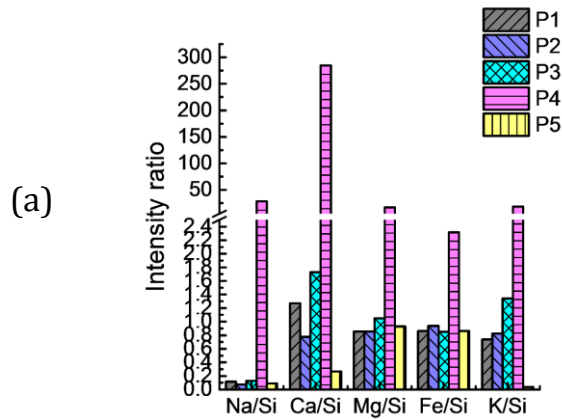
Figure 2.6   Samples elemental distribution as function of intensity ratio of Si.

From the 2D plot (Figure 2.6), it is observed that Mg/Si and Fe/Si are relatively constant in all samples except for starch (P4) whereas Ca/Si and K/Si vary throughout all the five samples. To better understand this relatively constant variation of the intensity of ratios, Mg/Si and Fe/Si in the talcum powders, we evaluated the standard deviations of the intensity ratios over talcum samples (P1, P2, P3 and P5) and reported this in Table 2.3.

Table 2.3 Intensity ratios of Na, Ca, Mg, Fe and K to Si in talcum (P1, P2, P3, and P5).

	P1	P2	P3	P5	SD	RSD
Na/Si	0.12	0.07	0.13	0.09	0.028	31.81
Ca/Si	1.27	0.78	1.73	0.26	0.633	67.70
Mg/Si	0.85	0.86	1.05	0.93	0.092	12.16
Fe/Si	0.86	0.94	0.85	0.86	0.042	5.91
K/Si	0.74	0.83	1.34	0.04	0.535	76.75

SD: standard deviation, RSD: relative standard deviation

From Figure 2.6 and Table 2.3, the high relative standard deviations for Ca/Si, K/Si, and to some extend Na/Si explain the variability of the concentration of these

42

elements in manufacturing baby powders. Mg/Si and Fe/Si, on the other hand, seem to vary little from sample to sample except in starch (P4). Considering the relative standard deviations of Fe/Si and Mg/Si ($\approx$5 and 13%, respectively) over samples (P1, P2, P3 and P5), these two ratios can be used to screen talc from starch. Although the present study is not about characterization of asbestos, our results appear similar to those of Caneve *et al*. [15] and Benton [16] on the characterization of pure asbestos. The similarity might stem from the fact that, talc (which might not be asbestos-free) is the primary raw material in most cosmetic baby powders. Observations from Figure 2.6 and Table 2.3 thus suggest that Si emission lines can be used as an internal standard to screen cosmetic powders by considering Mg/Si and Fe/Si ratios. Also, the low intensity ratios (Mg/Si and Fe/Si) can possibly be used as indicator of suspicious asbestos in talcum cosmetics, which will then require further investigation, with say transmission electron microscopy (TEM).

Multivariate principal component analysis

- To further our analysis of cosmetic powders, principal component analysis (PCA) was performed on the five sample sets. Using PCA to extract information from a data set consists of finding what makes samples different or similar to each other. Each sample in the data is seen as a point in a multidimensional space. In other words, the original variables (the spectral lines) are projected onto a smaller number of latent variables called principal components (PC). These projections give a better visualization of the information contained in the data. The principal components are iteratively computed such that the first PC carries most the information (most explained variance), the second PC carries the residual information not taken in account by the first PC, the third PC the residuals of the second PC, and so on. From these projections, the variance, loadings and scores plots are used to characterize the principal components. They provide information on the relative contribution of the various spectral lines being used. The variance gives an idea of the amount of information taken into account by each PC.

43

The spectral lines of all the fives samples were analyzed to obtain the most significant principal components. The scores and loadings plots reported in Figure 2.7 were generated using a multivariate analysis software, The Unscrambler X from Camo Inc.

Scores plot

Figure 2.7a illustrates the 2D scatter plot of the scores of the main principal components. It gives information about possible trends in the samples. From the scores plot (Figure 2.7a), two principal components are sufficient to explain our data set. The points plotted here represent the objects (that is the different samples). These two components together explain 98% variance of the collected emission spectra with PC1 representing 85% and PC2, 13%. In the scores plot, the talcum powders seem to have a vertical distribution along the axis of PC2. On the other hand, as we move from left to right of PC1,

44
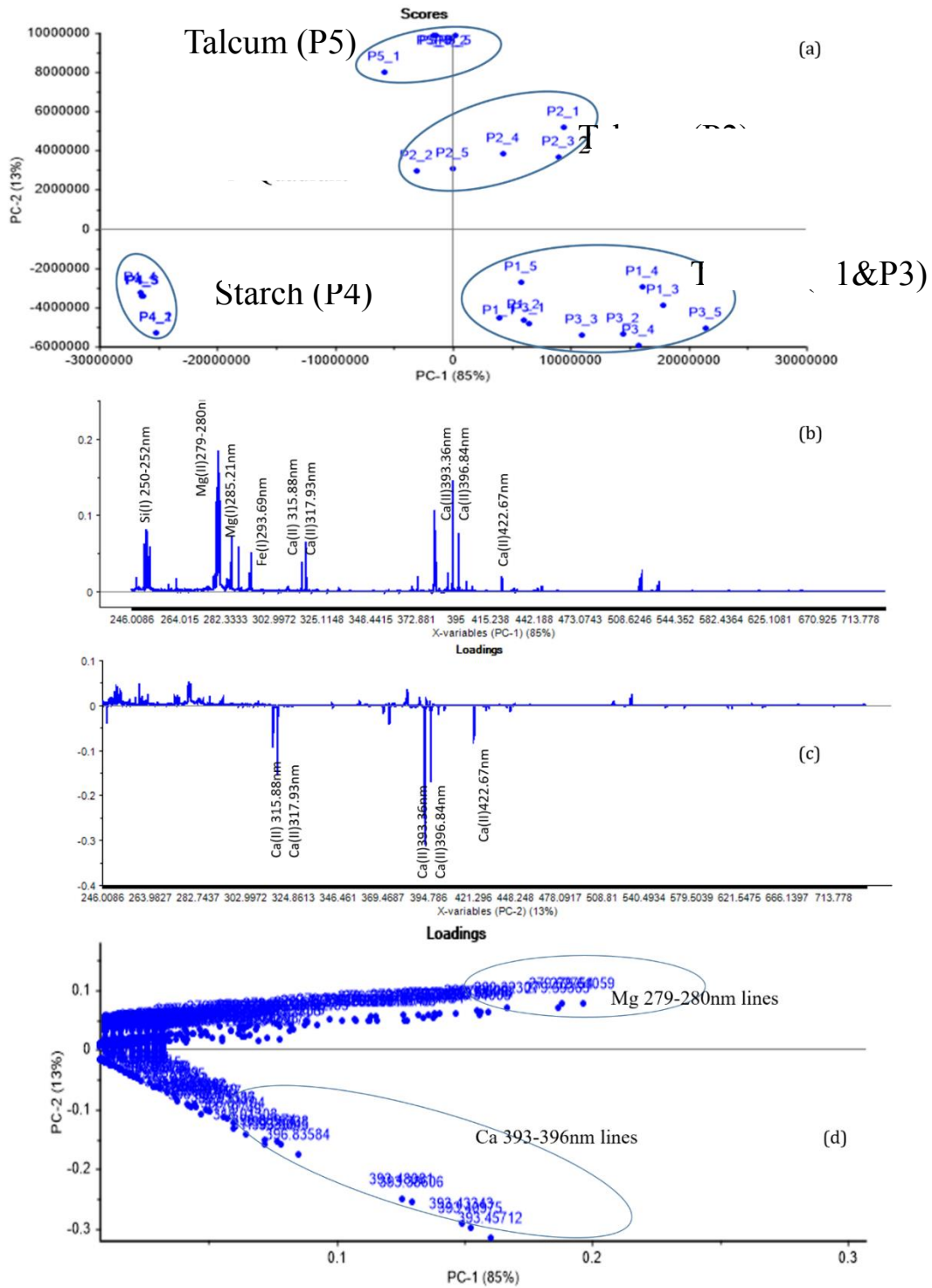
Figure 2.7   Principal component analysis results

(a) Scores plot, (b-c) line loadings plot for PC1 and PC2, (d) 2-D scatter loading plot of PC1 versus PC2.

45

we successively get P4 (the starch-based cosmetic), P5, P2 and (P1, P3) (talc-based cosmetics). Since P5, P2, P1 and P3 are all talc-based, their grouping in three sets suggests they have varying compositions of major constitutive elements (magnesium, calcium and silicon) with possible substitutes, such as aluminum observed in sample P5. This difference in composition might be understood from the loadings plots.

Loadings plot

The line loadings are shown in Figure 2.7 b,c. These loadings plots give insight about the variables behind the main differences between starch- and talc-based samples which could be used as screening factors.

For line loadings of PC1 (Figure 2.7b), we see that besides Mg, other elements such as Ca, Si and Fe also contribute more or less in characterizing our samples; this is the reason why we have up to 85% of the spectroscopic data explained by PC1. Previously in the scores plot, we observed that the sample were grouped horizontally from cornstarch (left) to talc-based (right). Since Mg has the highest contribution, we can attribute the grouping to Mg content. Thus, the principal component that carries the most information in our study is Mg and it is distributed along the PC1 axis. The other elements observed in the line loadings of PC1 could reflect the variant additives during the manufacturing process to substitute for Mg or Fe, as explained in the qualitative analysis section above.

On the other hand, looking at PC2 line loadings plot (Figure 2.7c), the only lines contributing are the calcium lines. Previously on the scores plot observation, we realized that there is a subgrouping within the talc-based cosmetics along the PC2 axis. Since for the PC2 loadings lines only Ca contributes, we can relate the subgrouping of talcum to

the content of calcium. Confirming the fact that talcum powders may contain variable amounts of associated minerals, such as calcite (calcium carbonate) and dolomite (calcium and magnesium carbonate) [2]. Finally, the 2D scatter loadings plot (Figure 2.7d) outlines the elements with highest contributions to PC1 and PC2, respectively. With Mg lines (279-280 nm) and Ca lines (393-396 nm) having the highest loading contributions to PC1 and PC2, respectively, the 2D scatter loading confirms the relationships made from the line loadings between PC1 and Mg on one hand and PC2 and Ca on the other.

Conclusions

Elemental composition analysis of cosmetic powders has been performed using laser induced breakdown spectroscopy. Because of the potential presence of asbestos in talc that may cause health problem, use of asbestos-free talc is encouraged. Nowadays on the market, an alternative raw material is used to replace talc in cosmetic products. The main objective of this study was to demonstrate the feasibility of rapid elemental analysis and screening of cosmetic powders based on the raw material used. Mg, Si, Ca, Fe, K and Na were qualitatively identified in all five samples with relatively different intensity strengths. Al was observed only in talcum sample (P5) and CN molecular band in starch sample (P4). Si was used as an internal standard to distinguish starch-based from talc-based products. The low intensity ratios of Mg/Si and Fe/Si in talcum powder could be used for fast screening and can be seen as an indicator of the potential presence of asbestos, for which a further analysis will be required. Principal component analysis further outlined the main variables responsible for the variance in the samples. Mg is linked to principal component PC1 (85% of the variance) and is the main element

47

responsible for the grouping of the samples into two sets (starch- versus talc-based). Ca which is linked to principal component PC2 (13% of the variance) is responsible for the subgrouping observed in talc-based sample as talcum powders may contain variable amounts of associated minerals, such as calcite (calcium carbonate) and dolomite (calcium and magnesium carbonate). In conclusion, the results show that LIBS can be used for rapid elemental analysis, screening and classification of cosmetic powders.

References

[1] D. Hahn and N. Omenetto, "Laser-induced breakdown spectroscopy (LIBS), part II: review of instrumental and methodological approaches to material analysis and applications to different fields," *Appl. Spectrosc.*, vol. 66, no. 4, pp. 347–419, 2012.

[2] "http://online6.edqm.eu/ep800/NetisUtils/srvrutil_getdoc.aspx/2L3WoDJa nCrmmD3CuHIveT6q0/0438E.pdf." .

[3] B. L. Harlow and P. A. Hartge, "A review of perineal talc exposure and risk of ovarian cancer," *Regul Toxicol Pharmacol*, vol. 21, no. 2, pp. 254–260, 1995.

[4] T. Yamamoto, A. Kida, Y. Noma, A. Terazono, and S. Sakai, "Development of a testing method for asbestos fibers in treated materials of asbestos containing wastes by transmission electron microscopy," *Waste Manag.*, vol. 34, no. 2, pp. 536–541, 2014.

[5] S. Karageorgi, M. A. Gates, S. E. Hankinson, and I. De Vivo, "Perineal Use of Talcum Powder and Endometrial Cancer Risk," *Cancer Epidemiol. Biomarkers Prev.*, vol. 19, no. 5, pp. 1269–1276, 2010.

[6] P. K. Mills, D. G. Riordan, R. D. Cress, and H. A. Young, "Perineal talc exposure and epithelial ovarian cancer risk in the Central Valley of California," *Int. J. Cancer*, vol. 112, no. 3, pp. 458–464, 2004.

[7] B. L. Harlow, D. W. Cramer, B. A. Bell, and W. R. Welch, "Perineal Exposure to Talc and Ovarian Cancer Risk," *Obstet. Gynecol.*, vol. 80, no. 1, pp. 19–26, 1992.

[8] D. M. Gertig, D. J. Hunter, D. W. Cramer, A. Graham, F. E. Speizer, C. Walter, and S. E. Hankinson, "Prospective Study of Talc Use and Ovarian Canver," *J. Natl. Cancer Inst.*, vol. 92, no. 3, pp. 249–252, 2000.

[9] J. Whysner and M. Mohan, "Perineal application of talc and cornstarch powders: evaluation of ovarian cancer risk.," *Am. J. Obstet. Gynecol.*, vol. 182, no. 3, pp. 720–724, 2000.

[10] Z. Ulanowski, P. Kaye, and E. Hirst, "Respirable asbestos detection using light scattering and magnetic alignment," *J. Aerosol Sci.*, vol. 29, no Supp. I, pp 13–14, 1998.

[11] E. Hirst, P. H. Kaye, and J. A. Hoskins, "Potential for recognition of airbone asbestos fibres spatial laser scattering profiles," *Ann. Occup. Hyg.*, vol. 39, no. 5, pp. 623–632, 1995.

[12]   C. Rinaudo, E. Belluso, and D. Gastaldi, "Assessment of the use of Raman spectroscopy for the determination of amphibole asbestos," *Mineral. Mag.*, vol. 39, no. 3, pp. pp. 455–465, 2004.

[13]   R. E. Gordon, S. Fitzgerald, and J. Millette, "Asbestos in commercial cosmetic talcum powder as a cause of mesothelioma in women," *Int. J. Occup. Environ. Health*, vol. 20, no. 4, pp. 318–332, 2014.

[14]   Y. Suzuki and S. R. Yuen, "Asbestos fibers contributing to the induction of human malignant mesothelioma.," *Ann. N. Y. Acad. Sci.*, vol. 982, pp. 160–176, 2002.

[15]   L. Caneve, F. Colao, F. Fabbri, R. Fantoni, V. Spizzichino, and J. Striber, "Laser-induced breakdown spectroscopy analysis of asbestos," *Spectrochim. Acta Part B At. Spectrosc.*, vol. 60, no. 7–8, pp. 1115–1120, 2005.

[16]   D. Benton, "Identification of Asbestos Using Laser-Induced Breakdown Spectroscopy: A Viable Alternative to the Conventional Approach?," *ISRN Spectrosc.*, vol. 2013, pp. 1–6, 2013.

[17]   J. D. Winefordner, I. B. Gornushkin, T. Correll, E. Gibb, B. W. Smith, and N. Omenetto, "Comparing several atomic spectrometric methods to the super stars: special emphasis on laser induced breakdown spectrometry, LIBS, a future super star," *Journal of Analytical Atomic Spectrometry*, vol. 19, no. 9, pp. 1061-1083, 2004.

[18]   D. Cremers and L. Radziemski, *Handbook of Laser–Induced Breakdown Spectroscopy,* 2nd ed. John Wiley & Sons, 2013.

[19]   R. Noll, *Laser-induced breakdown spectroscopy, fundamentals and applications*. Springer Berlin Heidelberg, 2012.

[20]   J. P. Singh and S. N. Thakur, *Laser-induced breakdown spectroscopy*. Elsevier, 2007.

[21]   A. Miziolek, V. Palleschi, and I. Schechter, *Laser Induced Breakdown Spectroscopy: Fundamentals and Applications*. Cambridge University Press, 2006.

[22]   F. Anabitarte, A. Cobo, and J. Lopez-Higuera, "Laser-induced breakdown spectroscopy: fundamentals, applications, and challenges," *ISRN Spectrosc.*, vol. 2012, pp. 1–12, 2012.

[23]   K. Y. Yamamoto, D. A. Cremers, M. J. Ferris, and E. F. Foster, "Detection of Metals in the Enviroment Using a Portable Laser-Induced Breakdown Spectroscopy Instrument," *Appl. Spectrosc.*, vol. 50, no. 2, pp. 222–233, 1996.

[24]   R. A. Multari, L. E. Foster, D. A. Cremers, and M. J. Ferris, "Effect of sampling geometry on elemental emissions in laser-induced breakdown spectroscopy," *Appl. Spectrosc.*, vol. 50, no. 12, pp. 1483–1499, 1996.

[25]   P. Fichet, P. Mauchien, and C. Moulin, "Determination of impurities in uranium and plutonium dioxides by laser-induced breakdown spectroscopy," *Appl. Spectrosc.*, vol. 53, no. 9, pp. 1111–1117, 1999.

[26]   B. Sallé, D. A. Cremers, S. Maurice, R. C. Wiens, and P. Fichet, "Evaluation of a compact spectrograph for in-situ and stand-off Laser-Induced Breakdown Spectroscopy analyses of geological samples on Mars missions," *Spectrochim. Acta - Part B At. Spectrosc.*, vol. 60, no. 6, pp. 805–815, 2005.

[27]   H. Suyanto, H. Kurniawan, T. J. Lie, and K. Kagawa, "Application of laser plasma confinement and bending effect for direct analysis of powder sample," *Spectrochim. Acta Part B At. Spectrosc.*, vol. 57, no. 8, pp. 1325–1332, Aug. 2002.

[28]   N. Idris, K. Kagawa, F. Sakan, K. Tsuyuki, and S. Miura, "Analysis of Heavy Metal Pollution in Soil Using Transversely Excited Atmospheric CO_2 Laser-Induced Plasma by Trapping the Soil in Microstructured Holes on Metal Subtargets," *Appl. Spectrosc.*, vol. 61, no. 12, pp. 1344–51, Dec. 2007.

[29]   Z. Lie, M. Pardede, and R. Hedwig, "Spectrochemical analysis of powder using 355 nm Nd-YAG laser-induced low-pressure plasma," *Anal. Bioanal. Chem.*, vol. 390, no. 7, pp. 1781–1787, Apr. 2008.

[30]   R. Hedwig and W. Budi, "Film analysis employing subtarget effect using 355 nm Nd-YAG laser-induced plasma at low pressure," *Spectrochim. Acta - Part B At. Spectrosc.*, vol. 61, no. 12, pp. 1285–1293, Dec. 2006.

[31]   D. Body and B. L. Chadwick, "Optimization of the spectral data processing in a LIBS simultaneous elemental analysis system," *Spectrochim. Acta - Part B At. Spectrosc.*, vol. 56, no. 6, pp. 725–736, 2001.

[32]   I. B. Gornushkin, P. E. Eagan, A. B. Novikov, B. W. Smith, and J. D. Winefordner, "Automatic correction of continuum background in laser-induced breakdown and Raman spectrometry.," *Appl. Spectrosc.*, vol. 57, no. 2, pp. 197–207, 2003.

[33]   I.B. Gornushkin, J.M. Anzano, L.A. King, B.W. Smith, N. Omenetto, and J.D. Winefordner, "Curve of growth methodology applied to laser-induced plasma emission spectroscopy," *Spectrochim. Acta Part B At. Spectrosc.*, vol. 54, no. 3–4, pp. 491–503, 1999.

51

[34] S. Clegg, E. Sklute, and M. Dyar, "Multivariate analysis of remote laser-induced breakdown spectroscopy spectra using partial least squares, principal component analysis, and related techniques," *Spectrochim. Acta - Part B At. Spectrosc.*, vol. 64, no. 1, pp. 79–88, Jan. 2009.

[35] K. K. Ayyalasomayajula, V. Dikshit, F. Y. Yueh, J. P. Singh, and L. T. Smith, "Quantitative analysis of slurry sample by laser-induced breakdown spectroscopy," *Anal. Bioanal. Chem.*, vol. 400, no. 10, pp. 3315–3322, Jul. 2011.

[36] C. B. Stipe, B. D. Hensley, J. L. Boersema, and S. G. Buckley, "Laser-induced breakdown spectroscopy of steel: a comparison of univariate and multivariate calibration methods.," *Appl. Spectrosc.*, vol. 64, no. 2, pp. 154–60, 2010.

[37] M. M. Tripathi, K. E. Eseller, F.-Y. Yueh, and J. P. Singh, "Multivariate calibration of spectra obtained by Laser Induced Breakdown Spectroscopy of plutonium oxide surrogate residues," *Spectrochim. Acta Part B At. Spectrosc.*, vol. 64, no. 11–12, pp. 1212–1218, 2009.

[38] J. W. B. Braga, L. C. Trevizan, L. C. Nunes, I. A. Rufini, D. Santos, and F. J. Krug, "Comparison of univariate and multivariate calibration for the determination of micronutrients in pellets of plant materials by laser induced breakdown spectrometry," *Spectrochim. Acta Part B At. Spectrosc.*, vol. 65, no. 1, pp. 66–74, 2010.

[39] S. Yao, J. Lu, K. Chen, S. Pan, J. Li, and M. Dong, "Study of laser-induced breakdown spectroscopy to discriminate pearlitic/ferritic from martensitic phases," *Appl. Surf. Sci.*, vol. 257, no. 7, pp. 3103–3110, 2011.

[40] Q. Godoi, F. O. Leme, L. C. Trevizan, E. R. Pereira Filho, I. A. Rufini, D. Santos, and F. J. Krug, "Laser-induced breakdown spectroscopy and chemometrics for classification of toys relying on toxic elements," *Spectrochim. Acta Part B At. Spectrosc.*, vol. 66, no. 2, pp. 138–143, 2011.

[41] K. H. Esbensen, D. Guyot, F. Westad, and L. P. Houmoller, *Multivariate data analysis in practice: an introduction to multivariate data analysis and experimental design. Multivariate Date Analysis*, 5th ed. 2004.

[42] T. R. Loree and L. J. Radziemski, "Laser-induced breakdown spectroscopy: Time-integrated applications," *Plasma Chem. Plasma Process.*, vol. 1, no. 3, pp. 271–279, 1981.

[43] "http://physics.nist.gov/PhysRefData/ASD/lines_form.html." .

[44]   E. Tognoni, V. Palleschi, M. Corsi, G. Cristoforetti, N. Omenetto, I. Gornushkin, B. W. Smith, and J. D. Winefordner, "From sample to signal in laser-induced breakdown spectroscopy: a complex route to quantitative analysis," in *Laser-Induced Breakdown Spectroscopy (LIBS)*, A. Miziolek, V. Palleschi, and I. Schechter, Eds. Cambridge University Press, 2006, pp. 122–170.

[45]   L. J. Radziemski, T. R. Loree, D. A. Cremers, and N. M. Hoffman, "Time-resolved laser-induced breakdown spectrometry of aerosols," *Anal. Chem.*, vol. 55, no. 8, pp. 1246–1252, 1983.

[46]   M. Gondal, M. Dastageer, and A. Naqvi, "Detection of toxic metals (lead and chromium) in talcum powder using laser induced breakdown spectroscopy," *Appl. Opt.*, vol. 51, no. 30, pp. 7395–7401, 2012.

[47]   Q. Ma and P. J. Dagdigian, "Kinetic model of atomic and molecular emissions in laser-induced breakdown spectroscopy of organic compounds," *Anal. Bioanal. Chem.*, vol. 400, no. 10, pp. 3193–3205, 2011.

[48]   M. Kraushaar, R. Noll, and H. U. Schmitz, "Slag analysis with laser-induced breakdown spectrometry.," *Appl. Spectrosc.*, vol. 57, no. 10, pp. 1282–1287, 2003.

[49]   H. K. Sanghapi, K. K. Ayyalasomayajula, F. Y. Yueh, J. P. Singh, D. L. McIntyre, J. C. Jain, and J. Nakano, "Analysis of slags using Laser Induced Breakdown Spectroscopy," *Spectrochim. Acta Part B At. Spectrosc.*, vol. 115, no. 1, pp. 40–45, 2015.

[50]   C. Chaleard, P. Mauchien, and N. Andre, "Correction of Matrix Effects in Quantitative Elemental Analysis With Laser Ablation Optical Emission Spectrometry," *Journal of Analytical Atomic Spectrometry*, vol. 12, no. 2. pp. 183–188, 1997.

[51]   J. Vrenegor, R. Noll, and V. Sturm, "Investigation of matrix effects in laser-induced breakdown spectroscopy plasmas of high-alloy steel for matrix and minor elements," *Spectrochim. Acta Part B At. Spectrosc.*, vol. 60, no. 7–8, pp. 1083–1091, 2005.

53

CHAPTER III

ANALAYSIS OF SLAG BY LASER-INDUCED BREAKDOWN SPECTROSCOPY[2]

Abstract

The feasibility of using laser-induced breakdown spectroscopy (LIBS) for the analysis of gasification slags was investigated by comparing LIBS results to the results of an ICP-OES analyzer. A small amount of slag sample was placed on a piece of double-sided adhesive tape, attached to a glass microscope slide and analyzed for Al, Ca, Fe, Si, and V which are major elements found in slags. The partial least squares regression (PLS-R) and univariate simple linear regression (SLR) calibration methods indicated that apart from V (accuracy up to $\pm$ 20%), the accuracy of analysis varies within 0.35-6.5% for SLR and 0.06-10% for PLS-R. A paired-sample t-test within the 95% confidence level yielded p-values greater than 0.05, meaning no appreciable statistical difference was observed between the univariate SLR with internal standardization and the multivariate PLS-R for most of the analytes. For the results obtained in this work, LIBS response varies depending on the element and the technique used for quantitative analysis. Simultaneous use of the univariate calibration curves with an internal standard (intensity ratio) and PLS regression in multi-elemental analysis can help reduce the matrix effect of

---

slags associated with their high variation in concentration. Overall, these results demonstrate the capability of LIBS as an alternative technique for analyzing gasification slags. Estimated limits of detection for Al, Ca, Fe, Si and V were 0.167, 0.78, 0.171, 0.243 and 0.01 wt%, respectively.

Introduction

Slag has been widely studied and has proven useful in many industrial applications such as steel production and gasification. Slag analysis in metallurgical production processes increase steel quality by optimizing the chemical composition of slag, because the composition of a steel melt is greatly influenced by chemical reactions within the melt that can be seen within the slag components [1][2][3]. Slag analysis is also of great importance in some gasification processes where carbon feedstocks are converted into electricity, chemical products and transport fuel [4][5]. Environmental and economic challenges posed by the use of coal as feedstock have called for alternatives, such as petroleum coke (petcoke), biomass, and mixtures [6][7]. Development of reliable gasification technology depends on a good understanding of the influence of the feedstock mineral impurities on slag formation. Slag chemistry directly affects gasifier performance and its service life because of continuous interactions with protective lining materials during gasification and the viscous nature of the slag at exit. In some cases, slag could also be reused as a feedstock [8]. Chemical analysis of these slags is often carried out using inductively coupled plasma - optical emission spectroscopy (ICP-OES) or simply ICP [9]. This technique requires time-consuming sample digestion and has imitations for the analysis of refractory samples, resulting in incomplete digestion. This technique is also limited by lack of inline capabilities and significantly slowing feedback;

this can impact quality and productivity as it takes more time to make process and batch adjustments. X-ray fluorescence spectroscopy (XRF) is currently the state-of-the-art measuring technique for slags, but the major difficulty with this technique is the well-known effects of absorption and/or enhancement related to the major element composition of samples and standards, as well as higher detection limits and the availability of suitable certified reference materials [10]. In order to reduce analysis time in favor of online analysis, there is a need to seek other analytical methods. Laser-based methods are of great interest for their simplicity and other features, such as non-contact measurements with the analyte, less destructive, high measuring speed, and little or no sample preparation. Laser-induced breakdown spectroscopy (LIBS) is a spectrochemical analytical technique with the aforementioned features which permits multi-elemental analysis. LIBS has gained a lot of attention during the recent years as its scope of applications include solid, liquid, and gas analysis. There are a plethora of publications and books that elaborate on this versatile technique [11][12][13]. LIBS has previously been applied to multi-elemental analysis of slag samples from a steel plant and the reported results were in agreement with XRF. Coefficient of determination R^2 of 0.99 for the main analytes Ca, Si and Fe of converter slag was achieved. Fast analysis of vacuum slag samples by LIBS demonstrated for the first time in the steel works near a vacuum degasser station was 80 s with feasible further reduction. A representative analysis of SiO_2, CaO and Al_2O_3 of production samples without any further preparation was shown successfully in spite of sample heterogeneity and variations in color, cracks and holes [1][14].

56

In the present work, considering the advantages offered by LIBS as mentioned above, the aim was to present LIBS as an alternative method of analyzing gasification slags by comparing LIBS results to those obtained by ICP-OES. Synthetic slags with chemistry falling within coal-petcoke mixed feedstock slags were prepared for the investigation. The elements under investigation are Al, Ca, Fe, Si and V.

Material and methods

Experimental setup

Figure 3.1 shows the experimental setup. A frequency doubled second harmonic Q-switched Nd:YAG laser (Quantel CFR400, 20 Hz, 7-ns pulse width, 6-mm diameter, 235 mJ maximum pulse energy) was used as an excitation source. A small amount of sample was applied to a double-sided piece of tape that had been adhered to a glass slide. Once the sample was scattered onto the slide, it was then placed on a rotating platform to ensure that the laser hit a fresh spot during each pulse. The laser beam was focused onto the sample surface through a 30-cm focal length quartz lens and a right-angle prism. Spectra were collected with an Andor broadband spectrometer (Mechelle ME5000, 200–975 nm spectral range) through a 100-μm diameter optical fiber equipped with a pickup lens (Ocean Optics Inc. (OOI) Part No.74-UV). The latter was placed 5 cm away from the sample and at 45^0 with respect to the beam axis. Andor Solis software was used for acquisition setup. The spectrograph was connected to a personal computer for data acquisition. All measurements reported herein were carried out with the same gate delay, gate width and laser pulse energy. These were, respectively, optimized to 3 μs, 10 μs and 67.5 mJ. All spectra correspond to the accumulation of 50 laser shots, with each striking a fresh surface by rotating the sample. The resulting resolved spectra are used for

57

qualitative and quantitative analysis. The plasma was characterized by evaluating the plasma electron density and temperature from the calcium emission lines. The analysis software packages (Unscrambler X 10.3, OriginPro 2015, Veusz1.23.1 and Excel 2013) were used for data analysis.
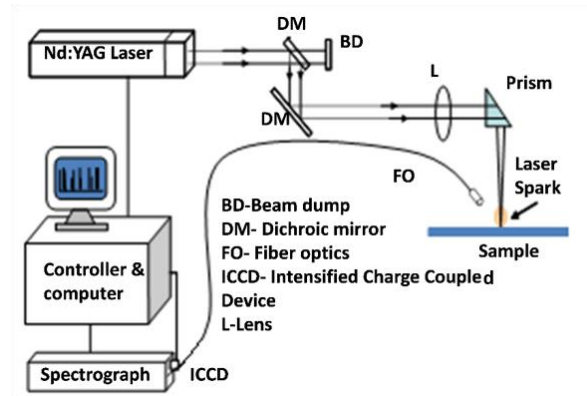
Figure 3.1   LIBS experimental setup for lag analyis.

Methods

The elemental compositions of slag samples are listed in Table 3.1.

Table 3.1 Elemental composition of samples.

Sample (wt.%)	Al	Ca	Fe	Si	V
S1	14.12	6.01	4.85	29.62	0.01
S2	10.55	6.26	2.64	35.11	0.93
S3	23.86	6.05	5.37	21.66	0.01
S4	9.66	6.01	2.54	31.97	2.90
S5	13.69	6.19	1.60	26.37	3.69
S6	15.10	5.61	2.57	22.49	6.38
S7	14.19	7.21	1.44	34.15	3.29
S8	12.49	5.84	2.21	31.71	0.01
S9	25.69	6.86	3.07	24.38	0.02
S10	25.95	7.42	4.51	24.24	6.07
S11	17.32	5.89	3.27	24.12	1.61
S12	19.03	6.60	3.05	25.55	4.19
T1	24.14	5.23	13.86	53.39	0.03
T2	20.93	5.09	12.45	47.07	10.97
T3	17.51	5.08	11.39	39.92	23.04
T4	9.68	5.25	8.32	27.28	46.65
T5	6.49	5.18	6.72	19.72	59.35

Concentration ranges of analytes in slag samples analyzed by ICP-OES.

Synthetic slags for this investigation were prepared following a procedure used by Nakano *et al.* [15]. Reagent grade powders of the respective oxides (Al, Ca, Fe, Si and V) were heated at 1425 °C for S1-7, 1575 °C for S8-12, and 1500 °C for the T1-5series in a 64 mol.% CO – 36 mol.% CO_2 atmosphere for 3 days, followed by water quench. Upon water quenching, all the molten slags were vitrified. The samples were then dried and ground into fine powders. For ICP analysis, a nominal mass of about 50 mg of the sample was fused with ~1g of $Li_2B_4O_7$ and diluted to a final volume of 100 mL using 5% HNO_3 [16]; the analysis was performed using spectral lines of Al 309.271 nm, Ca 317.933 nm, Fe 238.204 nm, Si 251.611 nm, and V 292.402 nm. External calibration and internal

59

standardization procedures [17] were utilized to quantify the analytes and based on a standard reference material (BIR-1). The accuracy of ICP analysis was within $\pm$ 7%. For LIBS analysis, about 10 mg of powder sample was placed on a double-sided adhesive tape glass slide.

Resuslts and discussion

Plasma characterization

Plasma parameters, such as temperature and electron density, were evaluated. The Boltzmann plot for calcium lines Ca(II) 396.84 nm, Ca(I) 430.25 nm, and Ca(I) 443.49 nm is shown in Figure 2.2. The spectroscopic data for these lines are given in Table 3.2.

Table 3.2 Spectroscopic data.

Lines	$g_i A_{ij}$	$E_i - E_j$	X_z	K_B	w
	$(x10^8 s^{-1})$	(eV)	(eV)	(eVK^{-1})	(nm)
Ca(II)396.84nm	0.70	0.00- 3.12			
Ca(I)422.67nm	6.54	0.00 - 2.93	6.11	$8.61x10^{-5}$	$4.84x10^{-4}$
Ca(I)430.25nm	2.72	1.89- 4.78			
Ca(I)443.49nm	1.34	1.88- 4.68			
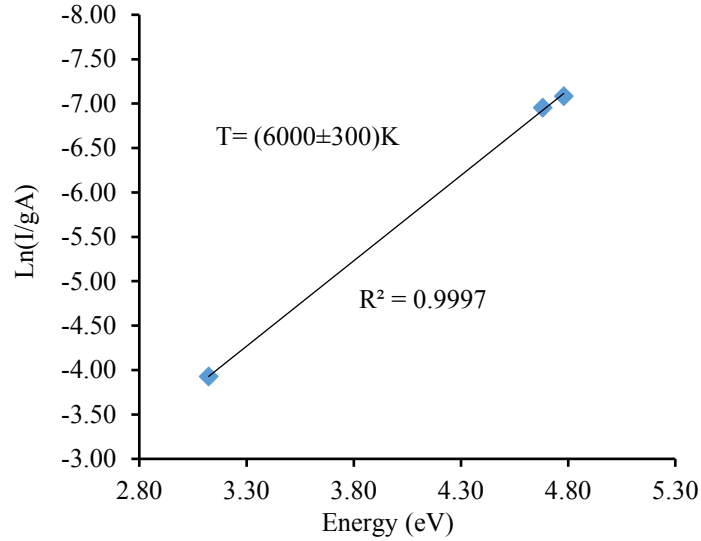
Figure 3.2   Boltzmann plot.

The plot yielded an electron temperature T_e= (6000±300) K. Different ionization levels were used in order to avoid lines with close excitation energies. This was to limit the effect of varying spectral response of the apparatus, as well as to minimize the sensitivity to small fluctuations in emission intensity [18]. Electron density of the laser-induced plasma ranged from 10^{16} to 10^{19} cm^{-3} and for this study, the electron density was determined from Stark broadening which avoids assumptions regarding local thermodynamic equilibrium (LTE) [18]. To determine the electron density of the plasma, the spectral emission line for Ca (422.67 nm) was fitted using a Lorentzian profile while the corresponding broadening coefficient at T=5000K was considered from Griem [19]. An average electron density N_e of 9.87×10^{17}cm^{-3}±4.67% was observed for all samples.

Quantitative analysis

Precision and accuracy of LIBS analysis are limited by matrix effects [11] [16]. Kraushaar *et al*. [1] observed that the variation in the major elemental composition of

61

slag leads to matrix effects. These observed variations ultimately affect the ablation rate, thus increasing the fluctuation in the emission lines and reducing the sensitivity of the instrument. Many studies have investigated matrix effects and its possible remedies using internal standardization and multivariate analysis [20][1][21][22]. In this chapter, internal standardization is used for univariate calibration with Ca and Si as internal standards whereas PLS-R calibration models are used for multivariate analysis, by considering the spectral range for each element (Al, Ca, Fe, Si and V). Due to the differences in concentration ranges, two sets of calibration curves were plotted. The first set included samples (S1-12) and the second set samples (T1-5). In the case of (S samples), 10 samples were used for calibration and 2 for predictions. For (T samples), 4 were used for calibration and 1 for predictions.

Univariate simple linear regression (SLR)

Univariate calibration curves for the two sets of data are shown in Figure 3.3 where intensity ratios are plotted against concentration ratios.
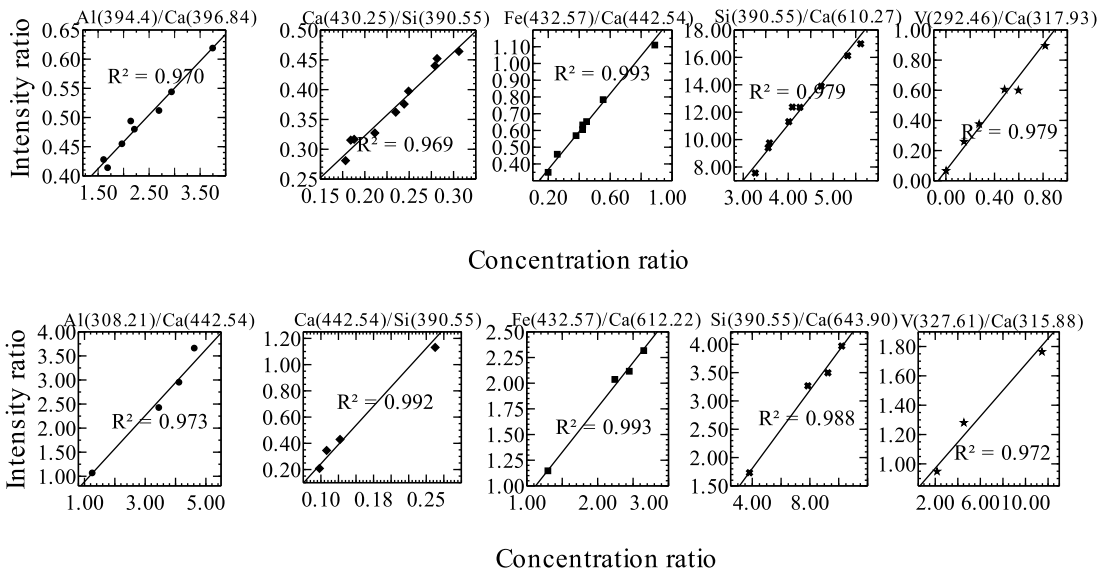
Figure 3.3   Simple linear calibration plots.
Top (Sample set S) and bottom (Sample set T)

Ca and Si were used as internal standards. Though the correlation coefficients R^2 are between 0.969 and 0.993, the best fit revealed the presence of outliers for certain elements, notably vanadium. This can be seen from the reduced number of plotted points (Figure 3.3) where only 6 out of 10 samples were used for the calibration of S samples and where only 3 of 4 samples were used for calibration of T samples. The presence of outliers can be attributed to the difficulties in minimizing shot to shot fluctuation in multi-elemental analysis of LIBS.

Multivariate partial least squares regression (PLS-R)

Figure 3.4 shows the PLS-R calibration models for Al, Ca, Fe, Si and V.

63
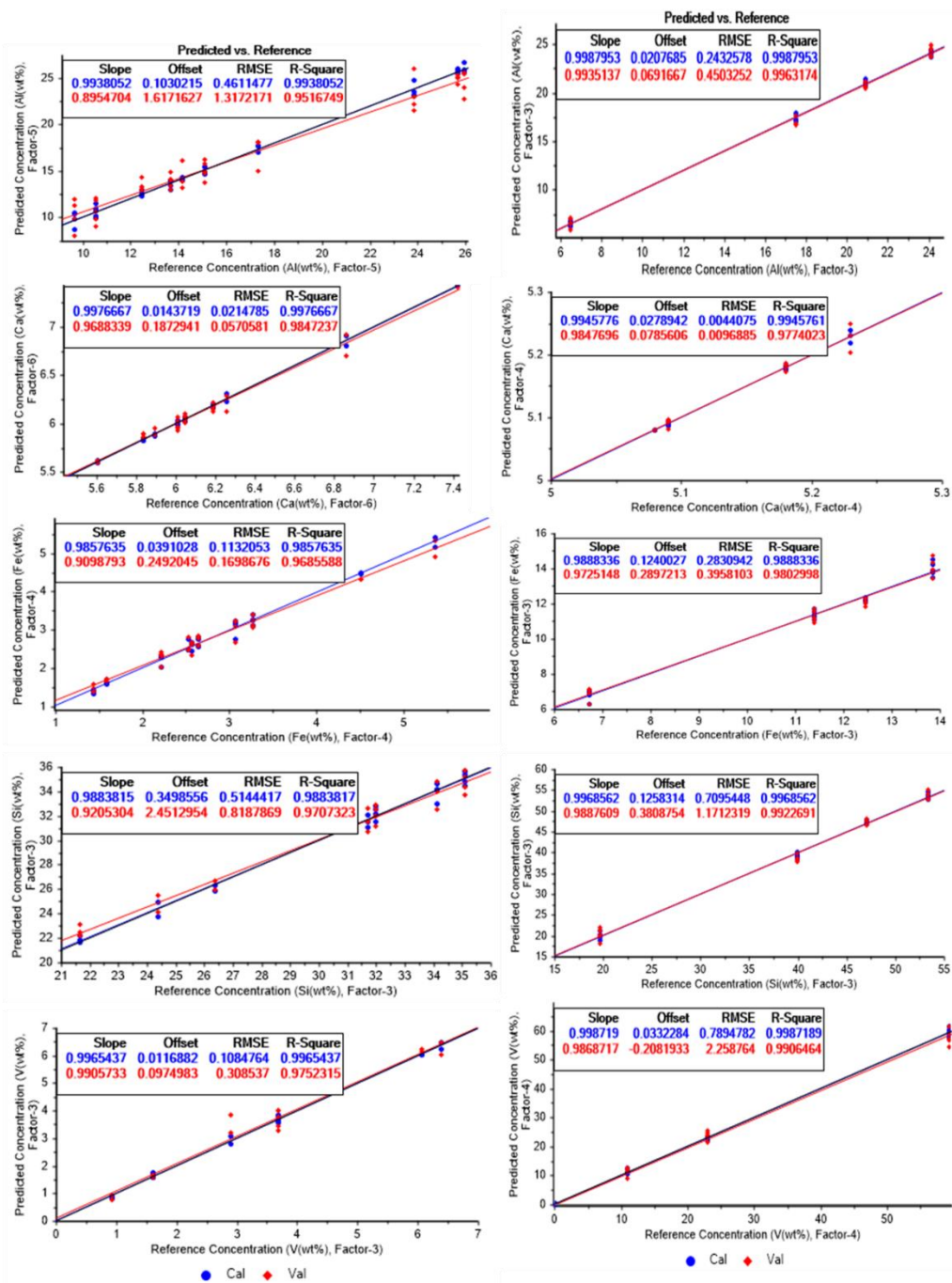
Figure 3.4   Partial least squares regression calibration.

• Cal and ♦ Val are the calibration and validation data, respectively.

It is observed that the R^2 values are almost equal to 1, revealing a strong correlation between the predictions and references. With slopes tending to 1 and validation (val) R^2 close to the calibration (cal) R^2, we can qualify this model as good enough for running our regression. Furthermore, calibration and validation best fits deviate very little from target line due to the high value of R^2. Like in the univariate analysis, higher outliers were observed in the PLS-R calibration curve for vanadium.

Analytical figures of merit

To evaluate the figures of merit of LIBS, predictive results from these two approaches are compared to those obtained by ICP-OES. Measurement precisions and % accuracy error are evaluated. An approximation of the detection limits is calculated.

Comparative results of partial least square, univariate calibration curves versus ICP

A comparison of LIBS and ICP results is shown in Figure 3.5.
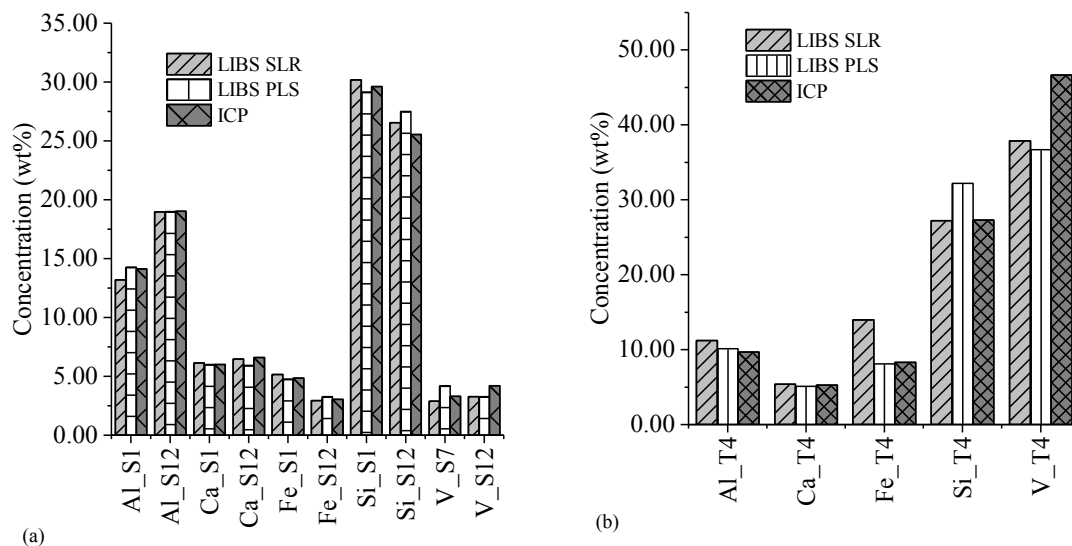
Figure 3.5   Comparison of LIBS (SLR&PLS-R) versus ICP-OES. (a) Sample set S and (b) Sample set T.

65

Predictions were done with sample S1, S7, S12 and T4. LIBS results were obtained with SLR and PLS-R and reported as the mean value of five measurements. In general, the repeatability for the major elements in terms of relative standard deviation (RSD) (Table 3.3) for SLR and PLS-R are almost on a par except for Al and Ca.

Table 3.3 Comparison of LIBS and ICP results.

|	LIBS (SLR)	LIBS (PLS)	ICP	RSD(%)		% Accuracy Error		Confidence & Significance level (95%, 0.05)	
	wt%			SLR	PLS	SLR	PLS	t Statistic	P value>|t|
Al_S1	13.20±1.91	14.27±0.71	14.12	14.49	5	6.49	1.1	1.95	0.12
Al_S12	18.96±1.98	18.99±0.17	19.03	10.42	0.9	0.35	0.19	0.03	0.98
Ca_S1	6.13±0.28	6.02±0.05	6.01	4.55	0.86	2.03	0.06	1.12	0.33
Ca_S12	6.48±0.33	5.92±0.07	6.6	5.14	1.2	1.85	10.24	3.51	0.03
Fe_S1	5.16±0.20	4.78±0.26	4.85	3.93	5.41	6.44	1.53	2.11	0.10
Fe_S12	2.93±0.05	3.26±0.13	3.05	1.84	3.94	3.65	7.07	8.04	<0.01
Si_S1	30.18±1.77	29.14±1.86	29.62	5.88	6.39	1.86	1.63	1.21	0.29
Si_S12	26.54±2.00	27.51±2.43	25.55	7.53	8.84	3.9	7.67	0.67	0.54
V_S7	2.88±0.42	4.19±0.45	3.29	14.61	10.8	12.47	27.61	4.66	0.01
V_S12	3.27±0.39	3.26±0.13	4.19	11.88	3.94	21.95	22.2	0.05	0.96
Al_T4	11.21±2.10	10.11±0.20	9.68	18.71	1.97	15.83	4.4	1.26	0.28
Ca_T4	5.39±0.34	5.12±0.07	5.25	6.33	1.3	2.58	2.57	1.94	0.13
Fe_T4	13.96±1.47	8.08±0.32	8.32	10.54	3.92	13.72	2.84	9.33	<0.01
Si_T4	27.22±3.74	21.18±3.74	27.28	13.74	11.63	0.24	17.96	2.22	0.09
V_T4	37.85±10.49	36.67±8.84	46.65	27.72	24.12	18.87	21.38	0.2	0.85

The percent accuracy error (Table 3.3) explains the deviation from the reference (ICP) values. Apart from V where the accuracy error is up to 20% for both SLR and PLS-R, the accuracy error is within 0.35-6% for SLR and 0.06-10% for PLS-R. Since the accuracy varies depending on the technique used, a paired-sample t-test was performed within the 95% confidence level in order to find the significance of the mean difference between SLR and PLS-R. Overall, the difference of the population means was not significantly different from the test difference as the p-values (Table 3.3) were greater than the significance level (0.05). This signifies that no appreciable statistical difference

was observed using univariate SLR calibration with internal standardization and the multivariate PLS-R except for Ca (S12), Fe (S12) Fe (T4) and V (S7). Using the reference (ICP) values and the accuracy error to interpret the p-values for these elements, SLR performed better than PLS-R for Ca (S12) and Fe (S12) while PLS-R performed better than SLR for Fe (T4). As for V (S7), the paired-sample test could not be validated based on the high accuracy error with respect to the reference value. With the exception of V for which the accuracy error is about ±20%, the use of internal standardization and multivariate analysis have resulted in accuracy of up to 0.06% for other elements. Simultaneous use of univariate calibration curves with internal standard and PLS regression in multi-elemental matrix demonstrates the capability of LIBS as an alternative technique for analyzing gasification slags.

Limit of detection

The limit of detection (LOD) defined as *3CN/I* can be calculated from a spectrum with lowest analyzed concentration, where *N* is noise calculated from the standard deviation of the background near the analyzed line; *C* is the concentration of the analyzed line; and *I* is the intensity of the analyzed line. The estimated limits of detection for Al, Ca, Fe, Si and V were 0.167, 0.78, 0.171, 0.243 and 0.01 wt%, respectively.

Conclusions

In this work, spectrochemical analysis of gasification slags has been reported using laser-induced breakdown spectroscopy (LIBS). Synthetic slags were prepared for investigating oxides of Al, Ca, Fe, Si and V. Quantitative analyses were performed using univariate calibration curves and partial least square regression (PLS). Internal

standardization was used in univariate (SLR) calibration curves to minimize the shot-to-shot variation in the plasma. LIBS results were compared with those obtained by ICP and they were in accordance. From the results obtained in this work, LIBS response varies depending on the element and the technique used for quantitative analysis. Thus, the simultaneous use of univariate calibration curves with internal standardization (intensity ratio) and PLS regression in multi-elemental analysis can help reduce the matrix effects of slags with high variation in concentration. Though the calibration curves might give a correlation coefficient greater than 0.95, it is worth performing predictions and evaluating the accuracy errors. Overall, these results demonstrate the capability of LIBS as an alternative technique for analyzing gasification slags.

References

[1]   M. Kraushaar, R. Noll, and H. U. Schmitz, "Slag analysis with laser-induced breakdown spectrometry," *Appl. Spectrosc.*, vol. 57, no. 10, pp. 1282–1287, Oct. 2003.

[2]   R. Noll, H. Bette, A. Brysch, M. Kraushaar, I. Mönch, L. Peter, and V. Sturm, "Laser-induced breakdown spectrometry — applications for production control and quality assurance in the steel industry," *Spectrochim. Acta Part B At. Spectrosc.*, vol. 56, no. 6, pp. 637–649, 2001.

[3]   V. Sturm, H. U. Schmitz, T. Reuter, R. Fleige, and R. Noll, "Fast vacuum slag analysis in a steel works by laser-induced breakdown spectroscopy," *Spectrochim. Acta Part B At. Spectrosc.*, vol. 63, no. 10, pp. 1167–1170, 2008.

[4]   M. Aineto, A. Acosta, J. Rincon, and M. Romero, "Thermal expansion of slag and fly ash from coal gasification in IGCC power plant," *Fuel*, vol. 85, no. 16, pp. 2352–2358, 2006.

[5]   M. Khosravi and A. Khadse, "Gasification of Petcoke and Coal/Biomass Blend: A Review," *Int. J. Emerg. Technol. Adv. Eng.*, vol. 3, no. 12, pp. 167–173, 2013.

[6]   S. Xu, Z. Zhou, X. Gao, G. Yu, and X. Gong, "The gasification reactivity of unburned carbon present in gasification slag from entrained-flow gasifier," *Fuel Process. Technol.*, vol. 90, no. 9, pp. 1062–1070, 2009.

[7]   T. Wu, M. Gong, E. Lester, F. Wang, Z. Zhou, and Z. Yu, "Characterisation of residual carbon from entrained-bed coal water slurry gasifiers," *Fuel*, vol. 86, no. 7–8, pp. 972–982, 2007.

[8]   C. Powell, J. Bennett, B. Morreale, and T. Gardner, "Addressing the materials challenges in converting biomass to energy," in *Ceramic Transactions*, vol. 224, pp. 377–385, 2011.

[9]   I. M. Potgieter, "Analysis of ferromanganese and ferromanganese slag by means of inductively coupled plasma optical emission spectrometry," *Appl. Spectrosc.*, vol. 55, no. 12, pp. 1682–1685, 2001.

[10]   A. G. Coedo and M. T. Dorado, "Approach to the Solution of Carbon Content Influence in the X-ray Fluorescence Analysis of Ferromanganese," *Applied Spectroscopy*, vol. 48, no. 6. pp. 695–698, 1994.

[11]   A. Ciucci, M. Corsi, V. Palleschi, S. Rastelli, A. Salvetti, and E. Tognoni, "New procedure for quantitative elemental analysis by laser-induced plasma spectroscopy," *Appl. Spectrosc.*, vol. 53, no. 8, pp. 960–964, 1999.

[12]   J. P. Singh and S. N. Thakur, *Laser-induced breakdown spectroscopy*. Elsevier, 2007.

[13]   D. Cremers and L. Radziemski, *Handbook of Laser–Induced Breakdown Spectroscopy,* 2nd ed. John Wiley & Sons, 2013.

[14]   V. Sturm, H. U. Schmitz, T. Reuter, R. Fleige, and R. Noll, "Fast vacuum slag analysis in a steel works by laser-induced breakdown spectroscopy," *Spectrochim. Acta Part B At. Spectrosc.*, vol. 63, no. 10, pp. 1167–1170, 2008.

[15]   J. Nakano, M. Duchesne, J. Bennett, K.-S. Kwong, A. Nakano, and R. Hughes, "Thermodynamic effects of calcium and iron oxides on crystal phase formation in synthetic gasifier slags containing from 0 to 27wt.% V_2O_3," *Fuel*, vol. 161, no. 1, pp. 364–375, 2015.

[16]   J. C. Jain, C. R. Neal, and J. M. Hanchar, "Problems Associated with the Determination of Rare Earth Elements of a 'Gem' Quality Zircon by Inductively Coupled Plasma-Mass Spectrometry," *Geostand. Newsl.*, vol. 25, no. 2–3, pp. 229–237, 2001.

[17]   M. A. Schneegurt, J. C. Jain, J. A. Menicucci, S. A. Brown, K. M. Kemner, D. F. Garofalo, M. R. Quallick, C. R. Neal, and J. F. Kulpa, "Biomass byproducts for the remediation of wastewaters contaminated with toxic metals," *Environ. Sci. Technol.*, vol. 35, no. 18, pp. 3786–3791, 2001.

[18]   E. Tognoni, V. Palleschi, M. Corsi, G. Cristoforetti, N. Omenetto, I. Gornushkin, B. W. Smith, and J. D. Winefordner, "From sample to signal in laser-induced breakdown spectroscopy: a complex route to quantitative analysis," in *Laser-Induced Breakdown Spectroscopy (LIBS)*, A. Miziolek, V. Palleschi, and I. Schechter, Eds. Cambridge University Press, 2006, pp. 122–170.

[19]   H. Griem, *Spectral Line Broadening by Plasmas*. Academic Press, New York, 1974.

[20]   C. Chaleard, P. Mauchien, and N. Andre, "Correction of Matrix Effects in Quantitative Elemental Analysis With Laser Ablation Optical Emission Spectrometry," *Journal of Analytical Atomic Spectrometry*, vol. 12, no. 2. pp. 183–188, 1997.

[21]   J. Vrenegor, R. Noll, and V. Sturm, "Investigation of matrix effects in laser-induced breakdown spectroscopy plasmas of high-alloy steel for matrix and minor elements," *Spectrochim. Acta Part B At. Spectrosc.*, vol. 60, no. 7–8, pp. 1083–1091, 2005.

70

[22] J. A. Aguilera, C. Aragón, V. Madurga, and J. Manrique, "Study of matrix effects in laser induced breakdown spectroscopy on metallic samples using plasma characterization by emission spectroscopy," *Spectrochim. Acta Part B At. Spectrosc.*, vol. 64, no. 10, pp. 993–998, 2009.

CHAPTER IV

DETERMINATION OF ELEMENTAL ANLYSIS OF SHALE ROCKS USING

LASER-INDUCED BREAKDOWN SPECTROSCOPY[3]

Abstract

In this study laser-induced breakdown spectroscopy (LIBS) is used for elemental characterization of outcrop samples from the Marcellus Shale. Powdered samples were pressed to form pellets and used for LIBS analysis. Partial least squares regression (PLS-R) and univariate calibration curves were used for quantification of analytes. The matrix effect is substantially reduced using the partial least squares calibration method. Predicted results with LIBS are compared to ICP-OES results for Si, Al, Ti, Mg, and Ca. As for C, its results are compared to those obtained by a carbon analyzer. Relative errors of the LIBS measurements are in the range of 1.7 to 12.6%. The limits of detection (LOD) obtained for Si, Al, Ti, Mg and Ca are 60.9, 33.0, 15.6, 4.2 and 0.03 ppm, respectively. An LOD of 0.4 wt% was obtained for carbon. This study shows that the LIBS method can provide a rapid analysis of shale samples and can potentially benefit depleted gas shale carbon storage research.

---

[3] Most of the content in this chapter has been adapted from *Spetrochemica Acta B Atomic Spectroscopy*, Volume 122, pages 9-14, Hervé K. Sanghapi, Jinesh Jain, Alexander Bol'shakov, Christina Lopano, Dustin McIntyre. "Analysis of slags using laser-induced breakdown spectroscopy." Copyright (2016) with permission from Elsevier.

Introduction

Shales are of interest in geochemical and geological investigations because they may host petroleum and natural gas. For example, oil shale contains solid bituminous material (called kerogen) that yields substantial amount of oil and combustible gas upon destructive distillation. The Marcellus Shale deposits in eastern United States are well known for a large amount of natural gas distribution sorbed in the shale and in cracks and pores. Organic-rich shale formations that have been depleted of hydrocarbons through a period of primary production are potential candidates for geologic storage of CO_2 [1][2], accompanied by enhanced gas recovery (EGR). Marcellus Shale is an ideal material to study the elemental profile because: 1) both CO_2 and natural gas (CH_4) adsorption/desorption seem to have a correlation with mineral composition of the rocks [3], 2) the rocks that contain higher amounts of carbon contents (organic material) have greater ability to generate natural gas and potentially a greater capacity of CO_2 storage [4],   and 3) environmental issues associated with shale retorting requires substantial monitoring and control of waste products [5]. Thus there are a number of applications that would benefit from *in situ* and/or rapid knowledge of the elemental composition of the shale rock.

The analytical techniques [6] used for elemental analysis of shale are instrumental neutron activation analysis (INNA), X-ray fluorescence (XRF), and inductively coupled plasma-optical emission spectroscopy (ICP-OES). INNA needs a large neutron reactor for irradiation and the method is inherently slow. Although XRF is a relatively fast technique, the analysis generally requires a larger sample size and the technique is known [7] to achieve poor detection limits, particularly for light elements.

73

ICP-OES [8] is commonly used for determination of elemental composition of shale. This technique requires time-consuming sample digestion and has limitations for the analysis of refractory samples, resulting in incomplete digestion. None of these techniques is suitable for the analysis of carbon, which is generally analyzed by using a number of other analytical techniques [6]. Herein, we propose laser induced breakdown spectroscopy (LIBS) as an alternative analytical technique for the analysis of metals and light elements, such as C.

LIBS is very robust for its simplicity and has successfully been used for multi-element analysis, including total carbon. It is advantageous to use LIBS because it enables a rapid *in situ* sample analysis with little or no sample preparation. The use of an echelle or multi-channel spectrometer gives a broader spectral range, allowing for multi-element analysis. Recently, Washburn [9] reported the use of LIBS for geochemical and mineralogical characterization of shale. The spectra from the beginning and the end of laser pyrolysis were used for qualitative analysis of Mg, Na, Li, K, Ca and H. No quantification of these elements was reported in his studies.

To the best of our knowledge, no quantitative analysis of the Marcellus Shale has been done using LIBS. In this chapter, I quantitatively determine the major elemental composition of shale rocks by laser-induced breakdown spectroscopy. In order to ascertain the quantitative capability of LIBS, our results are compared to those obtained by ICP-OES and a carbon analyzer. The elemental concentrations may be mathematically converted to oxide weight percent where necessary for certain geological interpretations.

74

Experimental set up and sample preparation

Ten outcrop samples from the Marcellus Shale [10] were used in this study. The powdered samples were pressed into 13-mm diameter pellets using approximately 8-ton pressure, 4 min of dwell time, and 2 min of release time. No binder was added to the pellets. These pelletized shale samples were labeled as S210 – S219.

Measurements were performed using a J200-EC LIBS instrument (Applied Spectra, Fremont, CA) configured with a 266-nm laser and a six-channel optical spectrometer coupled to gated CCD arrays for broadband spectral registration within 190–1040 nm at a resolution of about 0.1 nm. Laser pulse energy was 25 mJ; pulse duration was approximately 4 ns, while a flat-top shaped laser beam was collimated onto the sample to produce an ablation spot 150 μm in diameter. Laser pulse repetition frequency was 10 Hz. Temporal variation of the signal-to-noise ratio (SNR) and signal-to-background ratio (SBR) was used to optimize the gate delay. The gate delay with maximum SNR and SBR at 0.2 μs was used as the optimal gate delay for sensitive acquisition of both atomic and ionic lines of elements. The gate width was fixed at 1.05 ms. All measurements were performed in air at atmospheric pressure.

The samples were interrogated using a grid of 7×7 laser ablation spots, covering an overall area of 1.9×1.9 mm^2 on the surface of every pellet. Each spot of the grid was ablated with 10 laser pulses and the spectra acquired from these 10 pulses were accumulated. As a result of this interrogation, 49 individual spectra were collected from each sample. The analytical spectral lines are averaged over 49 spectra. These spectra were used to build a multivariate partial least squares model, in order to rectify inter-

75

sample differences while retaining inherent variability of the LIBS signal within every sample.

Results and discussions

Quantitative analysis

Quantification of elements is performed by producing calibration curves with use of simple linear regression (SLR) and multivariate partial least squares regression (PLS-R). The ten samples were divided into two sets, eight for the calibration and two for the prediction sets. It should be noted that some geological analyses may use the independent analyses of samples to generate the SLR and PLS models. To evaluate the figures of merit of LIBS, predictive results from these two approaches are compared to those obtained by ICP-OES and a carbon analyzer. Total carbon was analyzed using a CM5015 carbon dioxide coulometer (UIC, Inc.) equipped with a high-temperature combustion furnace. Detection limits of these elements are also calculated.

Spectral lines selection

From the collected spectra, we were able to identify some major elements in the Marcellus Shale, notably Al, Ca, Ti, Si, Mg and C. These elements corroborated with the previous findings of Heron *et al.* [11], Gladney *et al.* [12], and Boström and Bach [13] on rock characterization using neutron induced capture gamma ray spectroscopy, X-ray fluorescence, and inductively coupled plasma optical emission spectrometry. Lines with spectral interference and resonance lines were mostly avoided and preference was given to non-resonance lines [14]. Quite often, resonance lines are the most affected by self-absorption and self-reversal effects when the concentration or the laser pulse energy is

76

high. These effects are even more pronounced in solid samples than in liquids [15]. For quantitative analysis purposes, the following emission lines from these elements were selected: Al (308.21 nm, 309.27 nm), Ca (643.90 nm, 646.25 nm, 649.37 nm), Si (288.15 nm), Mg (285.21 nm), Ti (334.94 nm, 336.12 nm, 337.27 nm) and C (247.85 nm) were chosen for simple linear regression (SLR) calibration curves. It should be noted that these are all non-resonance lines except Al (308.21 nm) and Mg (285.21 nm).

Simple linear regression

Figure 4.1 shows univariate calibration curves of selected analyte lines from which linear regressions are performed for each of the elements using OriginPro 2015 software, manufactured by OriginLab Corporation, USA.
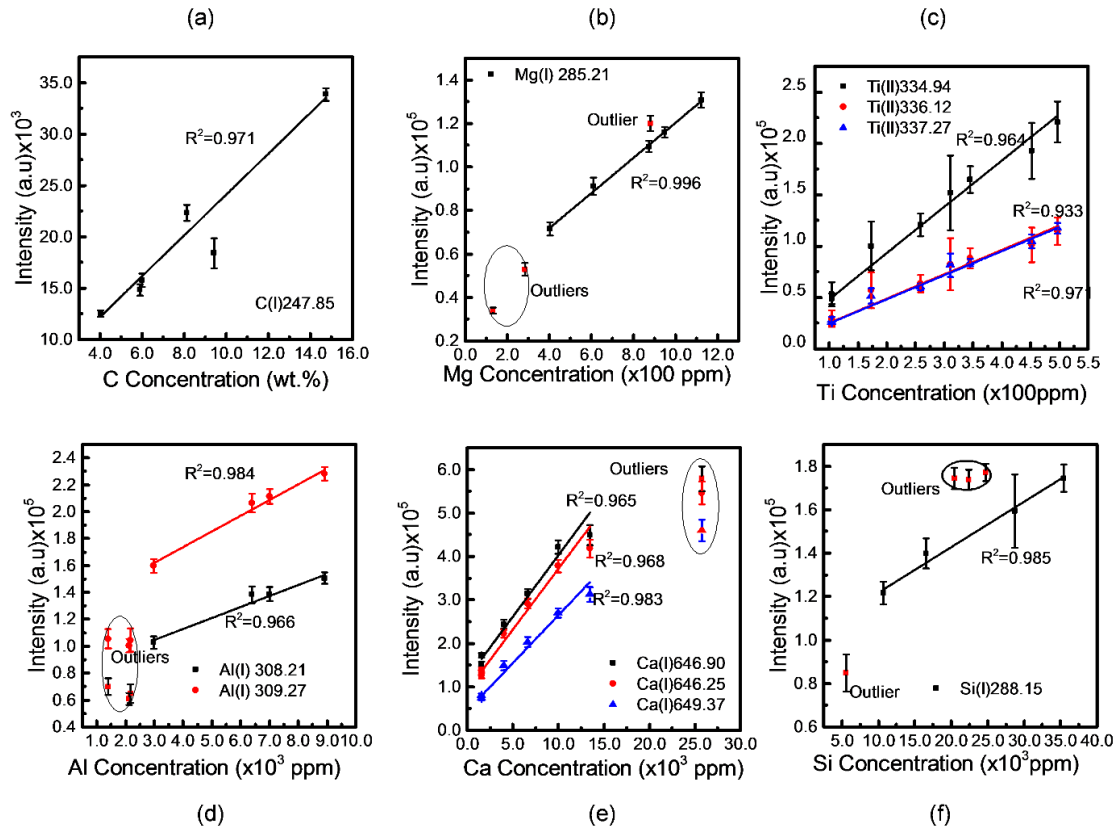
Figure 4.1   Simple linear regression calibration curves of selected analyte lines.

The linear regressions in Figure 4.1 show that R^2 is greater than 0.90, revealing a good correlation of the spectral lines and their concentrations. As seen in the plots in Figure 4.1, most of the calibration samples lie on the linear fit except for Al, Ca, Si and to a certain degree C where a few samples cluster away from the regression line and by this, reducing the linear dynamic range for these two elements. The data points lying far from the regression lines are likely outliers. However, the term "outlier" should be used with care. Although these outliers might just be statistical errors in data processing, judging from the relatively small variation of the error bars related to the intensity of these points, they might also be inherent in the very nature of the sample and the LIBS technique, in

78

which case we describe this as "matrix effect." By "matrix effect," we refer to the influence of the physical and chemical properties of the sample on the plasma excitation. Laser-sample interaction and matrix effect have been reported as the main causes of imprecision of LIBS [16]–[18]. Controllable variables including, but not limited to choice of analytical line, laser shot-to-shot variance, speed of sample movement, and detector settings (time delay and gate width) also affect quantitative analysis of LIBS [17][19]. Specific emphasis on chemical matrix effects has also being discussed by Eppler *et al.* [20] in studying the effects of chemical speciation and matrix composition on Pb and Ba detection in soil and sand samples using LIBS. They found that the chemical compound and sample composition strongly influence emission signals. Since shale rock is composed of different elements with varying concentrations, chemical matrix effects can as well be invoked as source of the outliers observed in the Al, Ca and Si plots (Figure 4.1, d-f) or spectral interference.

Use of internal standard to minimize matrix effects

The nonlinearity of the calibration curve in Figure 4.1 within certain ranges can also be due to inhomogeneity and multi-elemental content of the shale samples which can induce changes in the plasma excitation. In case the nonlinear calibration curve is due to these changes in excitation, Cremers and Radziemski [16] proposed the use of analyte signal ratioed to another element present in the sample to straighten out the curve. This is known as internal standardization.

In the Al curve (Figure 4.1d), a linear fit is only observed at high concentrations. The lost sensitivity at high concentrations is often due to self-absorption although saturation of the detector response may also be responsible [16]. At low concentrations,

79

non-resonance lines, such as Al (309.27 nm), are less sensitive to the detector response and if adjacent lines exist near it (which is the case with resonance line Al(308.21nm)), spectral interference is likely to occur. This might be the case between the aluminum doublets within the 308-309 nm spectral range. Consequently, the lines are probably broadened at low concentrations. An attempt to reduce the matrix effect observed in Figure 4.1d, f was done by normalizing Al and Si with Mg and Ti, respectively. Figure 4.2 shows the resulting calibration curves.
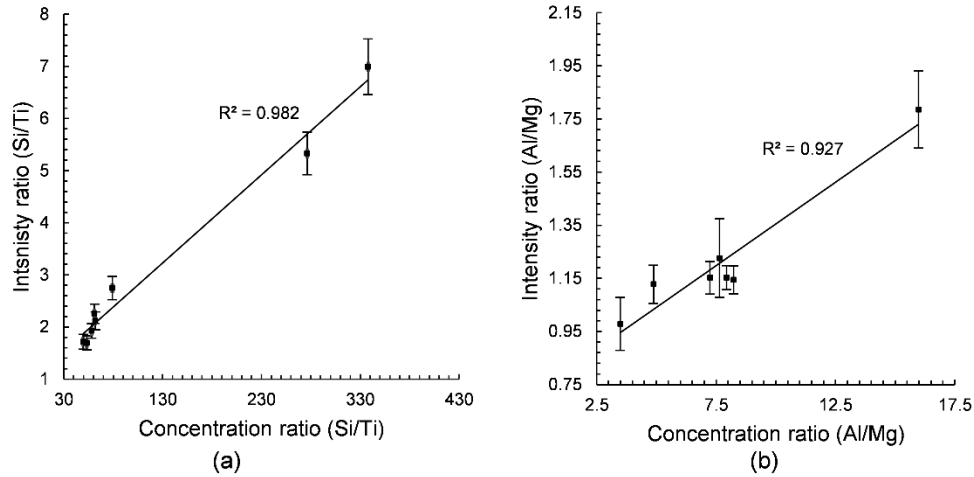
Figure 4.2   Calibration curve with internal standards. (a) Si (288.15 nm) / Ti (336.12 nm), (b) Al (308.21 nm)/Mg (285.15 nm).

Calibration curves with internal ratio show R^2 greater than that 0.90 over a wider linear dynamic range. In the case of Ca, no element used as an internal standard could yield a better graph. From the results of internal standardization, one can say that the outliers observed in Figure 4.1d and f and linked to the influence of other elements, notably Mg and Ti. As for Ca, it is probably related to its high concentration.

80

It follows that quantitative analysis of a matrix with multiple elements with varying and high concentrations can be affected by spectral interference; and the use of non-resonance lines and intensity ratios can help reduce the matrix effects and improve the quality of simple linear regression calibration curves.

Partial least squares regression

An alternative means of minimizing matrix effects is the use of multivariate analysis; this approach is especially useful when we have samples containing emission lines from multiple elements with high likelihood of strong spectral interferences. Multivariate analysis comes in various forms, amongst which is partial least squares (PLS) analysis. PLS has been widely used to minimize the matrix effect [21][22][23]. PLS provides a model for the relationship between a set of predictor variables X (n objects, m variables) and a set of response variables Y (n objects, p response). In this case, the m variables are the LIBS spectra intensities and the p responses are properties such as the concentration. The p response has to be independently measured for each sample. If the spectral data contain information about the properties of interest, a reliable calibration model can be constructed [24]. The samples with known elemental concentrations are used to create a model relating Y to X that is used to predict the concentrations of unknown specimens. PLS has the particularity of reducing the number of variables to a few principal components while taking into account the full spectrum of each sample. Each row of the data matrix X gives the wavelength-dispersed spectral intensities of one of the calibration samples, and these techniques seek to find a small number of principal component vectors (with the same dimension as the number of columns of X) upon which to base the regression. In the case of PLS, the principal

81

component vectors balance the importance of explaining the variance in X with that of creating a strong correlation with Y in the regression step described below. This balance results in a robust model with good predictive ability [25][26]. Although PLS often uses the full spectrum for models, some authors have proposed the use of proper selection of spectral ranges for better results when dealing with multi-elemental analysis. Xu and Schechter used an error indicator function of the net analyte signal to determine the analytical performance of an element in a certain spectral range [21]. Based on this, the most informative spectral ranges to be utilized in multicomponent analysis are selected [27]. Norgaard *et al.* have proposed interval partial least-squares (iPLS), which consists of developing local PLS models on equidistant subintervals of the full-spectrum region. This method provides an overall picture of the relevant information in different spectral subdivisions, thereby focusing on important spectral regions and removing interferences from other regions [28].

In the present study, the full spectrum was divided into reduced spectral ranges. The reduced spectral range was such that it contains most of the strong lines of a particular element (aluminum for example) for which we want to obtain the calibration curve. This procedure was repeated for others elements (Ca, Ti, Si, Mg and C). All recorded spectra were used to generate the partial least squares regressions using full cross validation on the average spectra. PLS-R were done with Unscrambler X version 10.3 software, from CAMO Software Inc, USA and the calibration and validation curves are shown in Figure 4.3.

82
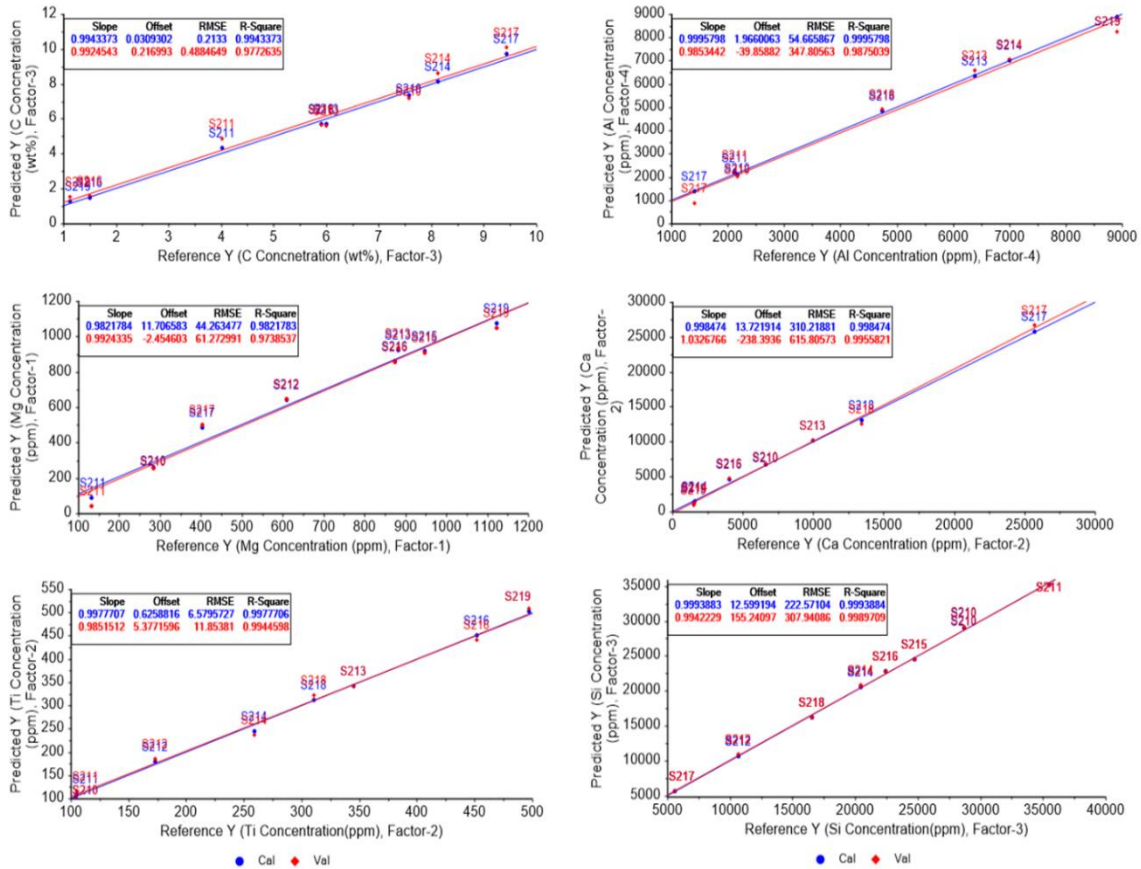
Figure 4.3   Partial least squares calibration curves for C, Al, Mg, Ca, Ti and Si.

In Figure 4.3, the best fit of the calibration and validation sets deviates slightly from the target line as seen from the values of the slopes which are almost equal to 1. The R^2 values are greater than or equal to 0.98. These observations show a strong correlation between the predicted and reference values over a wider linear dynamic range than for the univariate method.

Predictive capability of LIBS

The predicted concentrations using SLR and PLS-R in our study are compared with those from ICP-OES and a carbon analyzer. The results are reported in Table 4.1 and a comparison graph is plotted in Figure 4.4.

Table 4.1 Prediction results of LIBS and relative errors of determination.

Predictions Samples	Reference values	LIBS		Relative error (%)	
		SLR	PLS-R	SLR	PLS-R
(x100ppm)					
S215_Al	79.15	70.52	74.58	10.90	5.77
S216_Al	84.69	69.23	75.26	18.25	11.13
S218_Al	47.46	34.08	48.25	28.19	1.66
S212_Ca	171.78	167.48	156.73	2.50	8.76
S213_Si	180.54	308.46	197.74	70.85	9.52
S219_Si	246.88	433.66	235.63	75.65	4.55
S214_Mg	8.51	10.09	9.35	18.56	9.87
S218_Mg	9.33	8.27	8.25	11.36	11.57
S215_Ti	4.06	3.29	3.55	18.96	12.56
S217_Ti	0.96	1.38	0.52	43.75	45.83
(wt.%)					
S210_C	7.58	5.88	7.37	22.42	2.77
S215_C	3.56	-	3.98	-	11.79

Reference values were measured by ICP-OES (Al, Ca, Si, Mg, Ti) and
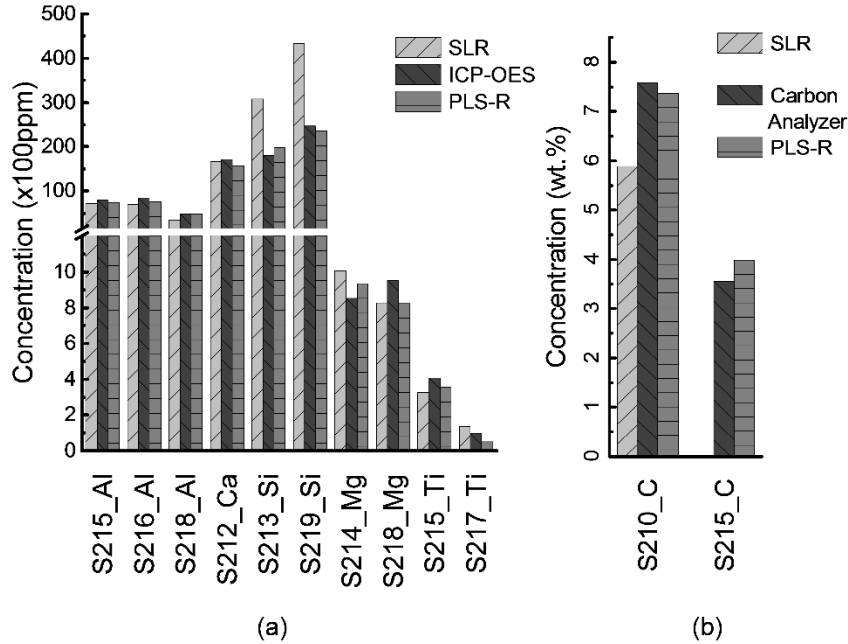carbon analyzer.

Figure 4.4   Comparison of LIBS (SLR and PLS-R) versus ICP-OES and carbon
            analyzer for Al, Ca, Mg, Si, Ti, and C.

In Table 4.1, a higher error is noted with SLR prediction of Si. This can be

understood from the silicate nature and inhomogeneity of shale rocks. In fact, studies on

silicate rocks have shown a high matrix effect of Si which interferes with Ti [29]. In

order to reduce the sample inhomogeneity, Claisse introduced borate glass [30] to obtain

highly reliable and precise results for XRF analysis of all rock types [31]–[33]. The

borate fusion method produces homogeneous samples that are easy to handle, can be

analyzed multiple times without deterioration, eliminate grainsize and mineralogical

effects, and reduce differences in mass absorption from sample to sample [34]. However,

LIBS presents a rather simple alternative, notably the possibility of avoiding sample

preparation, like the case of acid digestion, used to obtain homogeneity of a sample.

Although an attempt to reduce matrix effects was made with internal standardization, the

85

matrix effect is still present as seen from the SLR calibration. The use of multivariate

analysis has been preferred to minimize the matrix effect. In Table 4.1, the comparison

shows that the error for PLS-R (1.66 to 12.56%) for most elements is about half that of

SLR (2.50 to 75.65%). Figure 4.4 shows that LIBS results are comparable to those of

ICP-OES and a carbon analyzer.

Limit of detection

For each analyte, the spectrum with the lowest concentration was used to

calculate its limit of detection (LOD), which is defined as $LOD = 3\frac{c\sigma_s}{I}$, where c is the

lowest concentration, σ_s is the standard deviation of the background near the analyzed

line, and I the intensity (background subtracted) of the analyzed line. LODs for Al, Ca,

Si, Ti, Mg, and C are reported in Table 4.2.

Table 4.2   Calculated Limits of Detection (LOD).

Elements	LOD
Ti (II) 336.12 nm	15.6 ppm
Mg (I) 285.21 nm	4.2 ppm
Al (I) 309.27 nm	33.0 ppm
Si (I) 288.15 nm	60.9 ppm
Ca (I) 649.37 nm	0.03 ppm
C(I) 247.85 nm	0.4 wt.%

Conclusions

Laser-induced breakdown spectroscopy (LIBS) was used to determine the

elemental composition of Marcellus Shale rocks. Major elements (Al, Ca, Si, Mg, Ti, and

C) in shale rocks were qualitatively and quantitatively analyzed. Univariate calibration

(SLR) curves of Al, Ca, Si, Mg, Ti and C were compared to their corresponding

multivariate PLS-R calibrations. Quantitative analysis using PLS-R in LIBS helps

minimize the matrix effect and increase the linear dynamic range of concentration determination. LIBS offers the possibility of quantifying carbon, which is not possible for analysis by ICP-OES. Predicted results obtained by LIBS are similar to those obtained by ICP-OES for Al, Ca, Si, Mg and Ti and by a carbon analyzer for C. From our results and the advantages offered by LIBS (such as its simplified set up, cost and optical emission nature), we have demonstrated that the LIBS method can provide rapid analysis of shale rock samples.

References

[1] M. Godec, G. Koperna, R. Petrusak, and A. Oudinot, "Enhanced gas recovery and CO2 storage in gas shales: A summary review of its status and potential," *Energy Procedia*, vol. 63, pp. 5849–5857, 2014.

[2] B. C. Nuttall, C. F. Eble, M. R. Bustin, and J. A. Drahovzal, "Analyses of Devonian Black Shale in Kentucky for Potential Carbon Dioxide Sequestration and Enhanced Natural Gas Production.," Kentucky Geological Survey Report DE-FC26-02NT41442, 2005.

[3] H. T. Schaef, C. L. Davidson, A. T. Owen, Q. R. S. Miller, J. S. Loring, C. J. Thompson, D. H. Bacon, V. A. Glezakou, and B. P. McGrail, "CO2 Utilization and Storage in Shale Gas Reservoirs: Experimental Results and Economic Impacts," *Energy Procedia*, vol. 63, pp. 7844–7851, 2014.

[4] A. Busch, S. Alles, Y. Gensterblum, D. Prinz, D. N. Dewhurst, M. D. Raven, H. Stanjek, and B. M. Krooss, "Carbon dioxide storage potential of shales," *Int. J. Greenh. Gas Control*, vol. 2, no. 3, pp. 297–308, 2008.

[5] K. Piszcz, J. Luczak, and J. Hupka, "MOBILITY OF SHALE DRILL CUTTINGS," *Pysicochemical Probl. Miner. Process.*, vol. 50, no. 2, pp. 795–810, 2014.

[6] R. A. Nadkarni, "Analytical techniques for characterization of oil shales," *Am. Chem. Soc., Div. Pet. Chem., Prepr.;(United States)*, vol. 28, no. 1, 1983.

[7] P. M. Farkov, L. N. Il'icheva, and a. L. Finkel'shtein, "X-ray Fluorescence Determination of Carbon, Nitrogen, and Oxygen in Fish and Plant Samples," *J. Anal. Chem.*, vol. 60, no. 5, pp. 426–430, 2005.

[8] I. M. Potgieter, "Analysis of ferromanganese and ferromanganese slag by means of inductively coupled plasma optical emission spectrometry," *Appl. Spectrosc.*, vol. 55, no. 12, pp. 1682–1685, 2001.

[9] K. E. Washburn, "Rapid geochemical and mineralogical characterization of shale by laser-induced breakdown spectroscopy," *Org. Geochem.*, vol. 83–84, no. 1, pp. 114–117, 2015.

[10] C. W. Noack, J. C. Jain, J. Stegmeier, J. A. Hakala, and A. K. Karamalidis, "Rare earth element geochemistry of outcrop and core samples from the Marcellus Shale," *Geochem. Trans*, vol. 16, no. 6, pp. 1–11, 2015.

[11] M. M. Herron, M. E. Loan, A. M. Charsky, S. L. Herron, A. E. Pomerantz, and M. Polyakov, "Kerogen content and maturity, mineralogy and clay typing from drifts analysis of cuttings or core," *Petrophysics*, vol. 55, pp. 435–446, 2014.

[12]   E. S. Gladney, D. B. Curtis, and E. T. Jurney, "Multielement analysis of major and minor elements by thermal neutron induced capture gamma-ray spectrometry," *J. Radioanal. Chem.*, vol. 46, no. 2, pp. 299–308, 1978.

[13]   K. Boström and W. Bach, "Trace Element Determinaitons by X-ray Fluorescence Analysis : Advantages, Limitations, and Alternatives," *Proc. Ocean Drill. Program, Sci. Results*, vol. 142, pp. 61–68, 1995.

[14]   K. J. Grant, G. L. Paul, and J. A. O'Neill, "Quantitative elemental analysis of iron ore by laser-induced breakdown spectroscopy," *Appl. Spectrosc.*, vol. 45, no. 4, pp. p. 701–705, 1991.

[15]   J. P. Singh and S. N. Thakur, "Physics of Plasma in laser-Induced Breakdown Spectroscopy," in *Laser-Induced Breakdown Spectroscopy*, Elsevier, 2007, p. 94.

[16]   D. Cremers and L. Radziemski, *Handbook of Laser–Induced Breakdown Spectroscopy,* 2nd ed. John Wiley & Sons, 2013.

[17]   X. L. Mao, M. a. Shannon, A. J. Fernandez, and R. E. Russo, "Temperature and Emission Spatial Profiles of Laser-Induced Plasmas during Ablation Using Time-Integrated Emission Spectroscopy," *Appl. Spectrosc.*, vol. 49, no. 7, pp. 1054–1062, 1995.

[18]   J. A. Aguilera, C. Aragón, V. Madurga, and J. Manrique, "Study of matrix effects in laser induced breakdown spectroscopy on metallic samples using plasma characterization by emission spectroscopy," *Spectrochim. Acta Part B At. Spectrosc.*, vol. 64, no. 10, pp. 993–998, 2009.

[19]   I. Bassiotis and A. Diamantopoulou, "Effects of experimental parameters in quantitative analysis of steel alloy by laser-induced breakdown spectroscopy," ... *B At. Spectrosc.*, vol. 56, no. 6, pp. 671–683, 2001.

[20]   A. S. Eppler, D. A. Cremers, D. D. Hickmott, M. J. Ferris, and A. C. Koskelo, "Matrix effects in the detection of Pb and Ba in soils using laser-induced breakdown spectroscopy," *Appl. Spectrosc.*, vol. 50, no. 9, pp. 1175–1181, 1996.

[21]   J. Amador-Hernández, "Partial least squares regression for problem solving in precious metal analysis by laser induced breakdown spectrometry," *J. Anal. At. Spectrom.*, vol. 15, no. 6, pp. 587–593, 2000.

[22]   S. Clegg, E. Sklute, and M. Dyar, "Multivariate analysis of remote laser-induced breakdown spectroscopy spectra using partial least squares, principal component analysis, and related techniques," *Spectrochim. Acta - Part B At. Spectrosc.*, vol. 64, no. 1, pp. 79–88, 2009.

[23] S. Laville, M. Sabsabi, and F. R. Doucet, "Multi-elemental analysis of solidified mineral melt samples by Laser-Induced Breakdown Spectroscopy coupled with a linear multivariate calibration," *Spectrochim. Acta Part B At. Spectrosc.*, vol. 62, no. 12, pp. 1557–1566, 2007.

[24] M. Z. Martin, N. Labbé, T. G. Rials, and S. D. Wullschleger, "Analysis of preservative-treated wood by multivariate analysis of laser-induced breakdown spectroscopy spectra," *Spectrochim. Acta Part B At. Spectrosc.*, vol. 60, no. 7–8, pp. 1179–1185, Aug. 2005.

[25] H. Martens, *Multivariate Calibration*. John Wiley & Sons, 1992.

[26] C. B. Stipe, B. D. Hensley, J. L. Boersema, and S. G. Buckley, "Laser-induced breakdown spectroscopy of steel: a comparison of univariate and multivariate calibration methods.," *Appl. Spectrosc.*, vol. 64, no. 2, pp. 154–60, Mar. 2010.

[27] L. Xu and I. Schechter, "Wavelength Selection for Simultaneous Spectroscopic Analysis. Experimental and Theoretical Study," *Anal. Chem.*, vol. 68, no. 14, pp. 2392–2400, 1996.

[28] L. Norgaard, J. Wagner, J. P. Nielsen, L. Munc, and S. B. Engelsen, "nterval Partial Least-Squares Regression (iPLS): A Comparative Chemometric Study with an Example from Near Infrared Spectroscopy," *Appl. Spectrosc.*, vol. 54, no. 3, pp. 413–419, 2000.

[29] P. J. Potts, *A Handbook of Silicate Rock Analysis*. Springer Netherlands, 2013.

[30] F. Claisse, "Quebec Department of Mines.," PR 327, 1956.

[31] K. Norrish and B. W. Chappell, "X-ray fluorescence spectrometry," in *Physical Methods in Determinative Mineralogy*, Academic Press, London, 1967, pp. 161–214.

[32] K. Norrish and B. W. Chappell, "X-ray fluorescence spectrometry," in *Physical Methods in Determinative Mineralogy*, 2nd ed., Academic Press, London, 1977, pp. 201–272.

[33] K. Norrish and J. . Hotton, "An accurate X-ray spectrographic method for the analysis of a wide range of geological samples," *Geochim. Cosmochim. Acta*, vol. 33, no. 4, pp. 431–453, 1969.

[34] T. E. La Tour, "Analysis of Rocks Using X-Ray Fluorescence Spectrometry," *Rigaku J.*, vol. 6, no. 1, pp. 3–9, 1987.

CHAPTER V

LASER-INDUCED BREAKDOWN SPECTROSCOPY FOR QUANTITATIVE

ANALYSIS OF TRACE ELEMENTS IN HIGH PRESSURE CO_2 ENRICHED

WATER: AN APPLICATION TO CARBON SEQUESTRATION[4]

Objective

In the present chapter, we investigate laser-induced underwater plasma under high

CO_2 pressures. An underwater plasma is characterized in terms of electron density and

the experimental parameters (gate delay, laser energy) are optimized. The feasibility of

quantitative analysis of trace elements in CO_2-dissolved water under high pressure is

reported for application in the detection of CO_2 leakage during the carbon sequestration

process.

Introduction to carbon sequestration

For several decades, combustion of fossil fuels has raised environmental concerns

about the increase of anthropogenic emission of carbon dioxide (CO_2). This increase of

CO_2 enhances the greenhouse effect, leading to what is known as global climate change

[1][2]. With the ever increasing demand for energy, there is a need for alternative sources

of natural gas production and at the same time mitigating the greenhouse effect.

Renewable energy and nuclear energy are alternatives, but require advanced technology

---

[4] Ongoing work on underwater plasma review article with the participation of Christian Goueguel, Dustin
L. McIntyre, Jinesh Jain and Jagdish P. Singh.

for sustainable large scale production at affordable cost. Reduction of carbon dioxide remains the prime option to substantially circumvent deterioration of the ecosphere. A promising approach is Carbon Capture and Storage (CCS), which consists of trapping carbon dioxide at the source plant, compressing to supercritical fluid and storing in a well-selected site. Storage of CO_2, however, requires a careful selection of sinks that can securely store CO_2 for a considerable geological time without causing another major ecological concern. In view of this, different geological environments have been proposed [3][4].

Underground geological storage is a preferential means of storing CO_2 [4][5][6]. Depleted oil and gas reservoirs, coal formations, and deep saline aquifers can be used for storage of CO_2 [6]. Although carbon capture and storage has proven to be the best way of mitigating anthropogenic release of CO_2, it requires constant monitoring of the integrity of the storage because the risk of CO_2 leakage is real and can potentially impact groundwater resources. Also, a progressive leakage could eventually reach the deep waters where dissolved CO_2 will accumulate, resulting in a phenomenon similar to what happened in Lakes Monoun and Nyos in Cameroon in 1984 and 1986, respectively. In effect a sudden outburst of dissolved CO_2 was released, killing thousands of people and animals with serious impact on the ecosystem as well [7], [8].

In effect, dissolved CO_2 forms carbonic acid, which, in turn, increases the reactivity of the minerals in the geological formation. The interaction between the injected CO_2, the host rock, its embedded fluid, and the sealing cap-rock is thus susceptible to offsetting the geological, physical and chemical equilibria of the host rock, affecting its porosity and permeability and providing a pathway for CO_2 leakage [9].

92

Therefore, a careful selection and characterization of the potential storage sites is necessary and as is constant monitoring of its integrity as well.

Potential leakage can be predicted by monitoring the physical and chemical changes of the geological fluids. Subsurface fluid sample and tracer analysis have been used as CO_2 monitoring techniques [10][11]. In subsurface fluid sampling, liquid or gas samples are collected from the injection reservoir or the overlying formation. Information on physical and geochemical changes taking place in the reservoir due to CO_2 plume migration are then investigated to understand the fluid chemistry, CO_2 transport properties, and CO_2 saturation that are used to constrain reservoir simulation models. Subsurface tracer monitoring consists of tracking the migration of the CO_2 plume and assessing the phase partitioning of CO_2 in the reservoir. Sampling of the subsurface is, however, difficult because fluid mixtures, such as CO_2, brine, and hydrocarbons, density separate in the wellbore, temperature and solubility relationships change, and preserving samples at *in situ* temperature and pressure conditions is a major challenge [11]. Kuster flow-through samplers and Modular Formation Dynamics Testers are often used to retrieve and maintain samples at *in situ* pressure conditions. Freifeld [12] also developed a U-tube for down hole sampling. This instrument permits extraction and maintains the sample under *in situ* conditions. These methods are tedious and cannot be use as a standalone technology and analysis of major and minor elements is carried out in a laboratory with techniques such as mass spectrometry. Although, these methods of subsurface sampling give precision for alkalinity, pH, and real-time fluid gas compositions which are highly effective parameters to track the CO_2 plume [13], little attention has been afforded to the chemical analysis of trace elements in such

93

environments. By monitoring the variation of these trace elements in the presence of dissolved CO_2 at high pressure, one can predict changes in the chemical composition of a reservoir and by extension, the degradation of the of the storage site. For example, there has been concern about injecting CO_2 in a cement well because of the effect of carbonic acid on the walls. During the diffusion of the carbonated water into the cement matrix, $Ca(OH)_{2(s)}$ is dissolved by the acidic solution, which enhances leaching of Ca^{2+} out of the cement matrix; subsequently precipitation of $CaCO_{3(s)}$ in the cement matrix is observed as a result of Ca^{2+} diffusion [14]. Therefore, monitoring the variation of such elements in the site can be useful for monitoring the integrity of the geological site for carbon sequestration.

Spectroscopic study under high-pressure environment

Spectroscopic measurements have been used to determine solution composition under high-pressure and high-temperature conditions. For example, Sanchez-Valle *et al*. [15] used an externally heated diamond anvil cell and synchrotron X-ray fluorescence (SXRF) for *in situ* measurements of carbonate minerals (strontianite $SrCO_3$) at pressures up to 3.6 GPa and temperatures up to 523 K. Like mass spectrometry, SXRF is cumbersome with poor limit of detection (LOD) and is limited to analysis of light elements. Thus, there is need for an alternative technique with a simple configuration, that can provide lower limits of detection, cover a broader spectrum of elements, and perform *in situ* and real time analysis. Laser-induced breakdown spectroscopy (LIBS) offers such capabilities. Literature compiled in various textbooks shows that LIBS is a powerful analytical technique for elemental analysis with detection limits on the order of parts per million (ppm). It has been applied to solid, gaseous and liquid samples with

94

results comparable to those of standard analytical techniques, like ICP [16][17][18]. Due to its versatility, the LIBS technique has drawn more interest in various fields of applied sciences. The flexibility and the availability of field-portable devices, like the Chemcam [19], have seen LIBS being applied in harsh environments where real-time *in situ* monitoring is needed with little or no sample preparation. It has been deployed for environmental and geochemical applications for the analysis of natural fluids, minerals, rocks, soils, sediments, and other natural materials [20].

Underwater LIBS for bulk analysis

The interaction of high-power laser pulses with matter can lead to a dielectric breakdown through optical absorption, commonly referred to as laser-induced breakdown (LIB). This breakdown can be initiated through cascade ionization, which occurs with long pulse generation and needs seed electrons in the focal volume. In the short pulse regime, pure multiphoton ionization is generally predominant, where each molecule is individually ionized by the electric field without the need of seed electrons [21]. Laser-induced breakdown has led to a spectroscopic technique called Laser-Induced Breakdown Spectroscopy (LIBS). LIBS is an emission spectroscopy where optical emission lines (atomic, ionic, or molecular) are characteristic of the elements present in the sample and can provides both qualitative and quantitative analysis.

Despite the reported experimental investigations of breakdown in aqueous media [22][23], the theory behind the breakdown process remains less understood as compared with the case of solids and gases. The process is initiated by multiphoton ionization of the molecules in the focal volume. After this multiphoton ionization stage, a partially ionized plasma is formed. The resultant plasma reaches high temperature and pressure and finally

95

expands, which causes the creation of a shock wave and a cavitation bubble of vaporized gases. First on a picosecond timescale, the high-pressure shock wave travels at supersonic velocity from the breakdown site, quickly dampening to acoustic velocity. Then, the shock wave and the cavitation bubble continue to expand in a nanosecond timescale. Finally on a microsecond timescale, the cavitation bubble due to the liquid environment collapses and may release a second shock wave, depending on the laser pulse energy [21][23].

Even though LIBS has known considerable progress with solids and gaseous samples in a considerable number of publications [16][17][18], direct analysis of liquid samples is difficult, due to several inherent drawbacks, such as splashing, surface ripples, extinction of emitted intensity, and a shorter plasma lifetime [24]. The shock waves that ensued during vaporization of liquid samples increase the shot-to-shot variation and displacement of the plasma spot, thus lowering the reproducibility of the spectral measurements. On the other hand, splashing attenuates the incident laser light as well as the emission light from the created plasma. To overcome these short comings, various experimental LIBS setups have been devised among which include bulk analysis and dual-pulse excitation [25]. In dual-pulse excitation, the first pulse is used to ablate the material and the second pulse to further excite the resulting plasma and enhance the sensitivity of LIBS as well as the signal-to-noise ratio. However, for compactness and optical setup, a single pulse is often used. In this chapter, instead of initiating the plasma at the surface of the liquid, the plasma is initiated in the bulk of the liquid samples for underwater LIBS measurements.
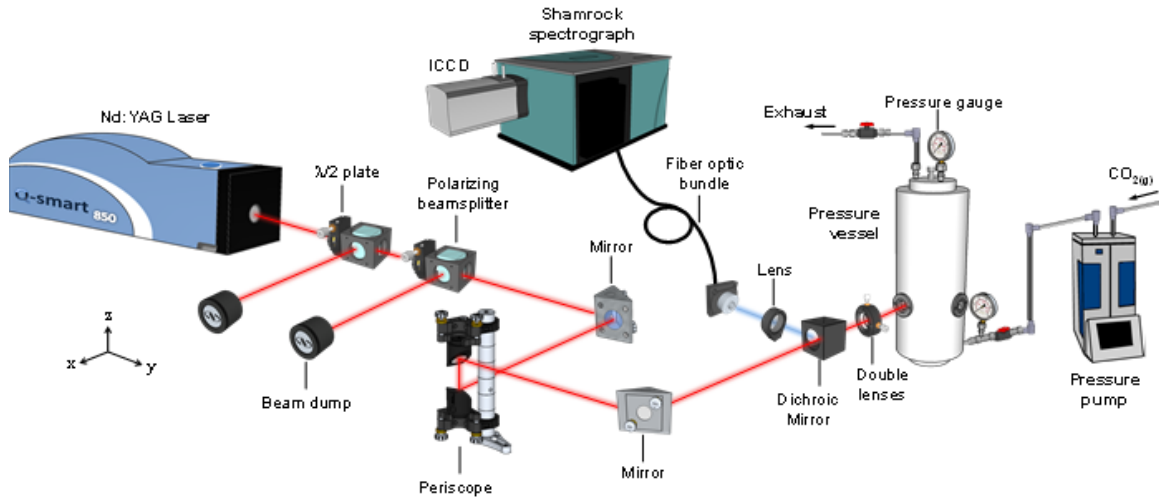
Experimental

Apparatus

Figure 5.1   An experimental setup for underwater LIBS.

Plasma creation in bulk liquid under high pressure dissolved gaseous CO_2 [9].

Our experimental setup is shown in Figure 5.1. A 1064-nm Q-switched Nd:YAG

laser (Q-smart 850, Quantel, 6-ns pulse width) was used as excitation source. A laser

with repetition rate was set to 5 Hz was used. Its beam was focused on the sample

through two UV-grade fused-silica plano-convex lenses of 100- and 80-mm focal length

and 25.4-mm diameter at a separation distance of 1 mm. A pair of half-wave plates and

polarizing beam splitters were used to attenuate the pulse energy. A high-energy

pyroelectric head detector (70273, Oriel Instruments) connected to a computer through an

Ophir compact Juno USB interface was used to control the pulse-to-pulse energy

variation. The liquid samples were put in 0.5-liter stainless steel high-pressure reactor

(Thar Technologies Inc.) and pressurized using a precision metering pump (QX-6000,

Ametek Inc.), set at a constant flow rate to inject CO_2. The pressure inside the reactor

97

was monitored using a high-speed USB output pressure transducer (PX409-5.0KGUSBH, Omega) attached to the reactor with a Swagelok fitting and using a laboratory-built LabVIEW program. A long-pass dichroic mirror (DMLP900, Thorlabs) and two UV-grade fused-silica plano-convex lenses of 40- and 10-mm focal length and 25.4-mm and 50mm diameter respectively were used to collect and focus the plasma light into a fiber bundle of 100-µm core diameter which is 2 m long (SR-OPT-8014, Andor Technology). This optical fiber was then connected to a Czerny-Turner spectrograph (Shamrock SR303i-A, Andor Technology) to record the plasma light emission in the form of spectra. The spectrograph signal was integrated with a 1024x256 pixels intensified charge-coupled device (ICCD) camera (DH320T-25F-03, Andor Technology). The gate delay was controlled with the built-in digital delay generator (DDG) of the spectrograph. The DDG is activated by the trigger pulse from the laser Q-switch output to synchronize data acquisition with the laser pulse [9].

Sample preparation

Solution sets of $CaCl_2$ were prepared by dissolving its powder form into pure water at various concentrations of Ca. Concentrations of calcium were 50, 100, 150, 200 and 300 ppm. Measurements of each solution were first carried under atmospheric pressure without CO_2 and later gaseous CO_2 was dissolved in the solutions at 5, 15 and 25 MPa pressure. The CO_2 used in this study was an industrial-grade gas.

Experimental conditions

As mentioned earlier, a plasma initiated in aqueous media is characterized by a shorter plasma lifetime. The displacement of the focal volume toward the laser, known as

98

moving breakdown, is often observed with a nanosecond laser. As a result of this, an elongated plasma is created, shielding points farther up the beam path, quenching the heating of the plasma, and causing an early decay of the plasma emission in this region [26]. Because of these, the intensity of the emission line is relatively low as compared to that of solid samples. In order to improve the strength of the emission intensity, we temporally resolved the LIBS spectra. Since laser pulse energy also plays a great role in initiating the breakdown in aqueous media, we also optimized the laser pulse energy.
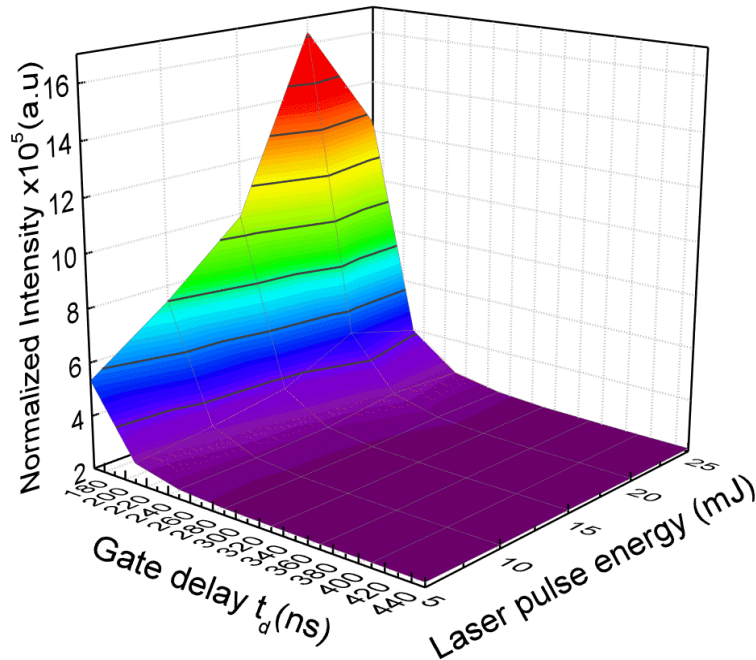

Figure 5.2   Normalized intensity of Ca line at 422.67 nm.

Figure 5.2 shows variation on the line intensity of a calcium line with respect to gate delay and laser pulse energy. It is observed that the line intensity decays fast after a couple hundred nanoseconds (around 250 ns). Also as the laser pulse energy increases, the intensity also increases, but drops after a certain value (20 mJ).

99

In order to obtain the best gate delay at which the analytical spectra will be collected, the signal-to-background ratio (SBR) is evaluated.
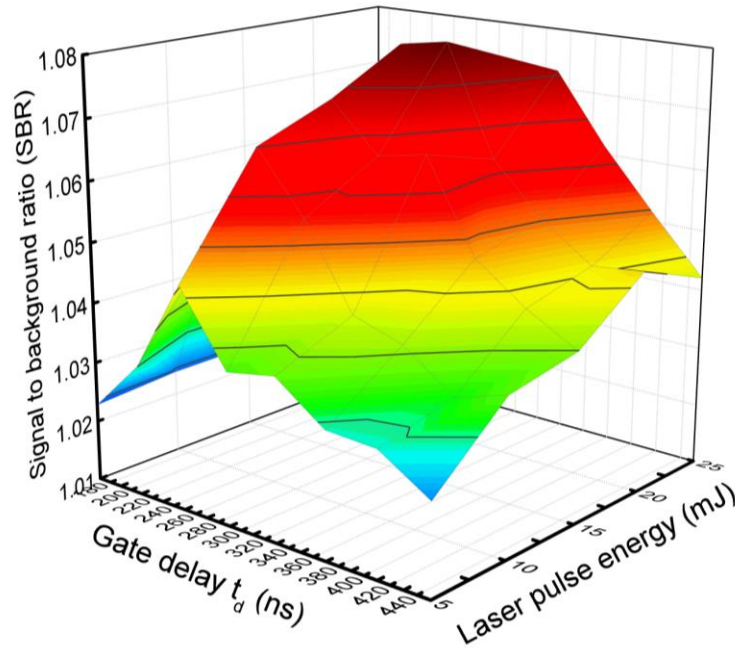

Figure 5.3   Signal-to-background ratio of Ca line at 422.67 nm.

In Figure 5.3, shows the variation of the SBR with respect to gate delay and laser pulse energy. It is observed that with the increase of laser pulse energy, the SBR increases as well and tends to be relatively constant after 20 mJ. However, with the various energies, SBR is optimum at 240-250 ns.

Results and discussion

Effect of pressure on line intensity

Selection of emission line plays an important role in obtaining good linear regression models from which quantitative results, such as the limit of detection, are derived. The concentration range is also taken into consideration when choosing lines. In

100

the case of high concentration, weak lines can be selected while resonance lines are used when the concentration is low. This choice is made to avoid self-absorbed and self-reversed lines and increases the linearity of the calibration curve [17]. However other factors, such as pressure, affects the emission lines through collisional (or pressure) broadening [16].
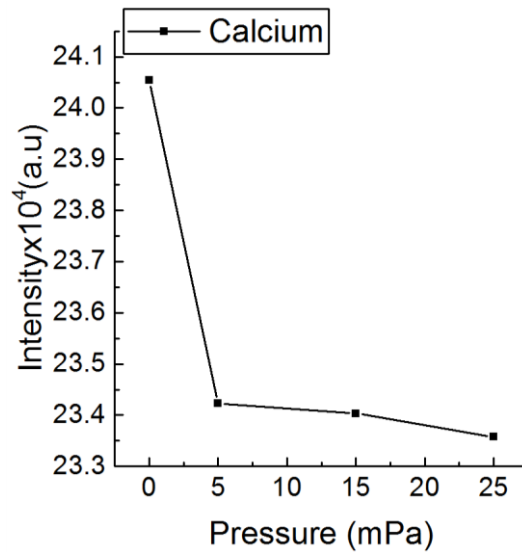

Figure 5.4   Variation of emission line intensity as function of pressure.

The effect of pressure on emission lines from underwater generated plasma is given in Figure 5.4. We used the calcium line at 396.84 nm. It is seen that the line intensity significantly drops when the environment of the generated plasma moves from atmospheric pressure to 5 MPa, after which an almost constant intensity is observed as the pressure increases. The drop in intensity can be related to spectral broadening due to pressure.

101

Effect of pressure on electron density

Quantitative analysis of LIBS greatly depends on the quality of the generated plasma. Plasmas should be optically thin, stoichiometric and in local thermodynamic equilibrium (LTE). In order to describe the characteristics of a plasma, parameters, such as the plasma electronic excitation temperature and the electron density, can be used. These can be obtained from the plasma emission data [17][18]. Figure 5.5 shows how the electron number density changes with increasing pressure.
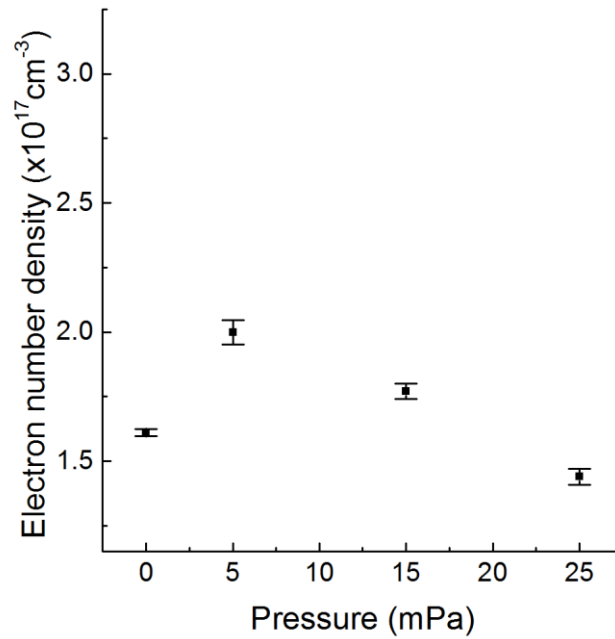

Figure 5.5   Evaluation of plasma electron number density as function of pressure.

The electron number density $N_e(cm^{-3})$ was evaluated using Stark broadening of a calcium line at 396.8 nm using the following equation [18]:

$$\Delta\lambda_{Stark} = 2w\left(\frac{N_e}{10^{16}}\right) \qquad (5.1)$$

where $\Delta\lambda_{stark}(nm)$ is the full-width-at-half-maximum (FWHM) obtained using a Lorentzian profile plot of the considered emission line, and $w(nm)$ is temperature dependent and represents the electron impact parameter referenced from Griem [27]. From Figure 5.5, we observed that the electron number density increases from atmospheric condition to 5 MPa, after which it starts to drop. This shows that at higher pressures of injected CO_2, the electron density is affected and this is due to the confinement of the plasma. The calculated electron number density falls within the reported literature range in LIBS, that is 10^{16} to 10^{19} cm-^{3} [28].

Quantitative analysis

As an analytical technique, LIBS aims at providing a quantitative result that can compete with other spectroscopic techniques such as inductively coupled plasma. This quantitative capability is often measured in terms of detection limit, that is the minimum measurable concentration. This is usually done by measuring the response of the system from which calibration curves are constructed. In LIBS, the system response is the measurement of the emission lines. Ideally, the response is linearly proportional to the concentration of the sample. Quantitative analysis of LIBS is however affected by factors such as the instability of the laser pulse energy. This experimental factor can be controlled or minimized by averaging recorded spectra. Other factors are inherent to the technique itself− principally the non-preparation of the sample which might enhance matrix effects due to the physical and chemical properties of the sample [17].

Calibration curves

The calibration curves for calcium emission lines at various pressures are shown in Figure 5.6.
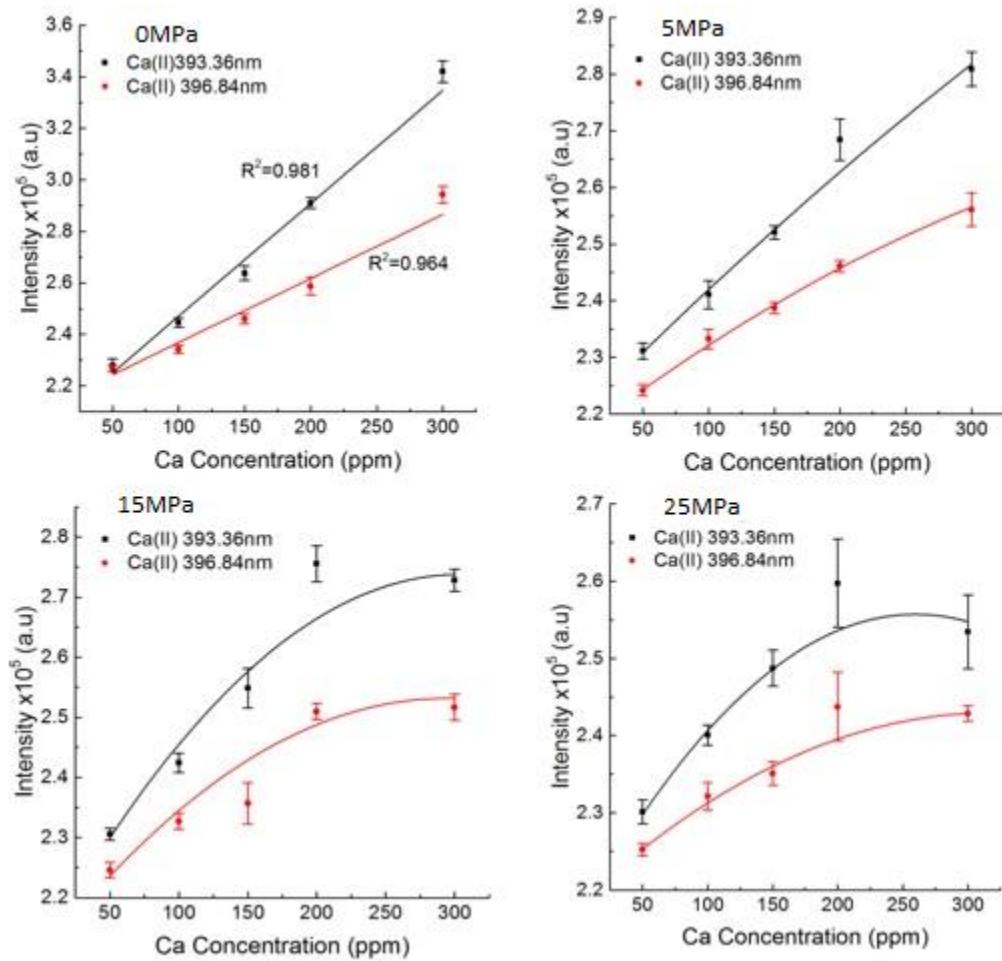

Figure 5.6　　Calibration curves of selected calcium lines.

The error bars in Figure 5.6 represents one standard deviation of five measurements. From Figure 5.6, it is seen that as pressure increases, not only the line intensity reduces, but also the linearity (dynamic ranges) drops slightly at 5 MPa and drops seriously afterwards. These results show the pressure dependence of the calibration

104

curves and the quantitative results, like detection limits, arising therefrom. At low pressures, increase of ablation is dominant due to reduced plasma shielding, which permits more absorption of laser pulse energy by the sample, therefore increasing the number of atoms in the plasma. However, this increases the number of collisions. A consequence of this collisional increase is the collisional broadening effect which distorts the shape of the spectral lines, thus reducing their emission line intensity [17].

Limit of detection

The limit of detection is evaluated according to the following equation

$$LOD = 3\frac{\sigma_B}{S} \qquad (5.2)$$

where σ_B is the standard deviation of background and S is the slope.

Table 5.1 Limits of detection (LOD) of calcium lines at different pressures of CO_2.

Emission line	Pressure of CO_2 (MPa)	LOD (ppm)
Ca(II) 393.36nm	0	17.26±0.24
	5	20.10 ±0.13
Ca(I) 396.84nm	0	15.49±0.33
	5	31.50±0.17

Reported limits of detection were limited to 5 MPa due to the limitation of the dynamic range at higher pressures of CO_2. Table 5.1 shows the detection limits of calcium in water under atmospheric pressure and under 5 mPa pressure of injected CO_2. It is seen that the as pressure of CO_2 increases, the detection limit increases as well. For calcium at 393.36 nm, the increase is not that much whereas at 396.84 nm the value practically doubles. This is explained by the loss of sensitivity observed in the calibration curve at 5 MPa (Figure 5.5) for Ca(II) 396.84 nm.

105

Conclusions

Experimental parameters, that is gate delay and laser pulse energy, have been investigated in view of quantitative analysis of trace elements in a high-pressure environment. Results show that pressure reduces the line intensity and to some extent that of the electron density. However, by temporally resolving the gate delay and optimizing the laser pulse energy, one can obtain underwater plasma emission with quantitative results on the order of 30 ppm within a certain limit of increased pressure. In effect the limit of detection increases as the pressure increases. Calibration curves show a loss of linearity with increase of pressure above 5 MPa. This study shows the possibility of using laser-induced breakdown spectroscopy to monitor the variation of trace elements. This can be applied in carbon sequestration. In effect, injected CO_2 enhances the acidity and thus favors more release of cations, like Ca^{2+}. So instead of measuring the carbon lines which is very difficult, one could rather monitor the variation of the trace elements to predict changes in the chemical composition of a reservoir and by extension the degradation of the of the storage site. This capability will be very beneficial to carbon sequestration technology.

Acknowledgement

References

[1] E. Bryant, "Climate process and change," Cambridge University Press, 1997, p. 209.

[2] C. J. Jepma and M. Munasinghe, "Climate change policy: Facts, issues and analyses Press," Cambridge University Press, 1998.

[3] S. Bachu, "Sequestration of CO_2 in geological media: Criteria and approach for site selection in response to climate change," *Energy Convers. Manag.*, vol. 41, no. 9, pp. 953–970, 2000.

[4] S. Bachu, "Sequestration of CO_2 in geological media in response to climate change: road map for site selection using the transform of the geological space into the CO_2 phase space," *Energy Convers. Manag.*, vol. 43, no. 9, pp. 87–102, 2002.

[5] S. M. Benson, "Carbon Dioxide Capture and Storage in Underground Geologic Formations," 1980, pp. 1–19.

[6] Sa. Benson P. Cook, J. Anderson, S. Bachu, H.B. Nimir, B. Basu, J. Bradshaw, G. Deguchi, J. Gale, G. von Goeme, and W. Heidug, , "Underground geological storage," *IPCC Special Report on Carbon Dioxide Capture and Storage*, vol. chapter 5, pp. 196–276, 2005.

[7] H. Sigurdsson, J. D. Devine, F. M. Tchua, F. M. Presser, M. K. W. Pringle, and W. C. Evans, ""Origin of the lethal gas burst from Lake Monoun, Cameroun," *J. Volcanol. Geotherm. Res.*, vol. 31, no. 1, pp. 1–16, 1987.

[8] G. E. Sigvaldason, "International conference on Lake Nyos disaster, Yaoundé, Cameroon 16– 20 March, 1987: conclusions and recommendations," *J. Volcanol. Geotherm. Res.*, vol. 39, no. 2, pp. 97–107, 1989.

[9] C. L. Goueguel, J. C. Jain, D. L. McIntyre, C. G. Carson, and H. M. Edenborn, "In situ measurements of calcium carbonate dissolution under rising CO_2 pressure using underwater laser-induced breakdown spectroscopy," *J. Anal. At. Spectrom.*, vol. 31, no. 7, pp. 1374-1380, 2016.

[10] M. Zhang and S. Bachu, "Review of integrity of existing wells in relation to CO2 geological storage: What do we know?," *Int. J. Greenh. Gas Control*, vol. 5, no. 4, pp. 826–840, 2011.

[11] "Monitoring , Verification , and Accounting of CO 2 Stored in Deep Geologic Formations – 2012 Update," *DOE/NETL-2012/1568*.

[12] B.M. Freifeld, "The U-tube: A new paradigm for borehole fluid sampling," *Sci. Drill.*, no. 8, pp. 41–45, 2009. LBNL paper LBNL-3741E.

[13] Y. K. Kharaka, D. R. Cole, S. D. Hovorka, W. D. Gunter, K. G. Knauss, and B. M. Freifeld, "Gas-water-rock interactions in Frio Formation following CO2 injection: Implications for the storage of greenhouse gases in sedimentary basins," *Geology*, vol. 34, no. 7, pp. 577–580, 2006.

[14] B. G. Kutchko, B. R. Strazisar, D. A. Dzombak, G. V. Lowry, and N. Thauiow, "Degradation of well cement by CO2 under geologic sequestration conditions," *Environ. Sci. Technol.*, vol. 41, no. 13, pp. 4787–4792, 2007.

[15] C. Sanchez-Valle, I. Martinez, I. Daniel, P. Philippot, S. Bohic, and A. Simionovici, "Dissolution of strontianite at high P-T conditions: An in-situ synchrotron X-ray fluorescence study," *Am. Mineral.*, vol. 88, no. 7, pp. 978–985, 2003.

[16] J. P. Singh and S. N. Thakur, *Laser-induced breakdown spectroscopy*. Elsevier, 2007.

[17] D. Cremers and L. Radziemski, *Handbook of Laser–Induced Breakdown Spectroscopy,* 2nd ed. John Wiley & Sons, 2013.

[18] A. Miziolek, V. Palleschi, and I. Schechter, *Laser Induced Breakdown Spectroscopy: Fundamentals and Applications*. Cambridge University Press, 2006.

[19] S. Maurice, R. C. Wiens, M. Saccoccio, B. Barraclough, O. Gasnault, O. Forni, N. Mangold, D. Baratoux, S. Bender, G. Berger, J. Bernardin, M. Berthé, N. Bridges, D. Blaney, M. Bouyé, P. Caïs, B. Clark, S. Clegg, a. Cousin, D. Cremers, a. Cros, L. Deflores, C. Derycke, B. Dingler, G. Dromart, B. Dubois, M. Dupieux, E. Durand, L. D'Uston, C. Fabre, B. Faure, a. Gaboriaud, T. Gharsa, K. Herkenhoff, E. Kan, L. Kirkland, D. Kouach, J. L. Lacour, Y. Langevin, J. Lasue, S. Le Mouélic, M. Lescure, E. Lewin, D. Limonadi, G. Manhès, P. Mauchien, C. McKay, P. Y. Meslin, Y. Michel, E. Miller, H. E. Newsom, G. Orttner, a. Paillet, L. Parès, Y. Parot, R. Pérez, P. Pinet, F. Poitrasson, B. Quertier, B. Sallé, C. Sotin, V. Sautter, H. Séran, J. J. Simmonds, J. B. Sirven, R. Stiglich, N. Striebig, J. J. Thocaven, M. J. Toplis, and D. Vaniman, "The ChemCam instrument suite on the Mars Science Laboratory (MSL) rover: Science objectives and mast unit description," *Space Sci. Rev.*, vol. 170, no. 1, pp. 95–166, 2012.

[20] R. S. Harmon, R. E. Russo, and R. R. Hark, "Applications of laser-induced breakdown spectroscopy for geochemical and environmental analysis: A comprehensive review," *Spectrochim. Acta Part B At. Spectrosc.*, vol. 87, no. 1, pp. 11–26, 2013.

[21] E. Abraham, K. Minoshima, and H. Matsumoto, "Femtosecond laser-induced breakdown in water: Time-resolved shadow imaging and two-color interferometric imaging," *Optics Communications*, vol. 176, no. 4. pp. 441–452, 2000.

[22]   D. X. Hammer, R. J. Thomas, G. D. Noojin, B. A. Rockwell, P. K. Kennedy, and W. P. Roach, "Experimental investigation of ultrashort pulse laser induced breakdown thresholds in aqueous media," *IEEE J. Quantum Electron.*, vol. 32, no. 4, pp. 670–678, 1996.

[23]   P. K. Kennedy, "A First-Order Model for Computation of Laser-Induced Breakdown Thresholds in Ocular and Aqueous Media: Part I—Theory," *IEEE J. Quantum Electron.*, vol. 31, no. 12, pp. 2241–2249, 1995.

[24]   D. M. D. Pace, C. A. D. Angelo, D. Bertuccelli, and G. Bertuccelli, "Analysis of heavy metals in liquids using Laser Induced Breakdown Spectroscopy by liquid-to-solid matrix conversion," vol. 61, no. 8, pp. 929–933, 2006.

[25]   D. A. Cremers, L. J. Radziemski, and T. R. Loree, "Spectrochemical Analysis of Liquids Using the Laser Spark," *Appl. Spectrosc.*, vol. 38, no. 5, pp. 721–729, 1984.

[26]   P. K. Kennedy, D. X. Hammer, and B. A. Rockwell, "Laser-induced breakdown in aqueous media," *Prog. Quantum Electron.*, vol. 21, no. 3, pp. 155–248, 1997.

[27]   H. Griem, *Spectral Line Broadening by Plasmas*. Academic Press, New York, 1974.

[28]   E. Tognoni, V. Palleschi, M. Corsi, G. Cristoforetti, N. Omenetto, I. Gornushkin, B. W. Smith, and J. D. Winefordner, "From sample to signal in laser-induced breakdown spectroscopy: a complex route to quantitative analysis," in *Laser-Induced Breakdown Spectroscopy (LIBS)*, A. Miziolek, V. Palleschi, and I. Schechter, Eds. Cambridge University Press, 2006, pp. 122–170.

CHAPTER VI

SUMMARY AND RECOMMENDATION FOR FUTURE

In this chapter I summarize the work covered throughout this dissertation and suggest future research.

Research summary

In this dissertation, my main focus was to use laser-induced breakdown spectroscopy to simultaneously analyze samples with more than one element and to applied it to investigate its application to some geological environments. Also in most cases, my quantitative results were compared with those of inductively coupled plasma-optical emission spectroscopy (ICP-OES).

In Chapter 2, laser-induced breakdown spectroscopy was used on various cosmetic powders. Principal component analysis was used to outlined the main variables responsible for the variance in the samples. Mg is linked to principal component PC1 (85% of the variance) and is the main element responsible for the grouping of the samples into two sets (starch- versus talc-based). Ca was associated with principal component PC2 and is responsible for the subgrouping observed in talc-based sample as talcum powders may contain variable amounts of associated minerals. The use of Si as internal standard aided distinguishing starch-based from talc-based products. It was also found that Mg/Si and Fe/Si have lower intensity ratios in talcum powder than in starch.

110

In Chapter 3, quantitative analysis of slags was reported using univariate calibration curves and partial least square regression (PLS). Internal standardization was used in univariate (SLR) calibration curves to minimize the shot-to-shot variation in the plasma. Results from LIBS were compared with those of ICP-OES. From the results obtained in this work, LIBS response varies depending on the element and the technique used for quantitative analysis; thus the simultaneous use of univariate calibration curves with internal standardization and PLS regression in multi-elemental analysis can help reduce the matrix effects of slags with high variation in concentration.

Geological samples, notably shales, were analyzed using LIBS for the first time in Chapter 4. Elemental composition of shales was thus reported. The quantitative results of major elements (Al, Ca, Si, Mg, Ti, and C) were again compared with those of ICP-OES. It was shown that using PLS-R with LIBS helps minimize the matrix effect and increase the linear dynamic range of concentration determination. LIBS offers the possibility of quantifying carbon, which is not possible for analysis by ICP-OES.

Quantitative analysis of trace elements from laser-induced underwater plasmas was investigated in Chapter 5. The effect of pressurized CO_2 on the line intensity and the plasma electron density was also investigated. Results show that pressure reduces the line intensity and to some extent the electron density. Optimizing the gate delay and the laser pulse energy showed that one can obtain underwater plasma emission with quantitative results on the order of 30 ppm. This study shows the possibility of using laser-induced breakdown spectroscopy to monitor the variation of trace elements in the presence of injected CO_2, which favors more release of Ca^{2+} due to the increase of acidity. This can be applied to carbon sequestration. Instead of measuring the carbon lines which is very

difficult one could rather monitor the variation of the trace elements to predict the changes in the chemical composition of a reservoir and by extension the degradation of the of the storage site.

Recommendation for future research

Herewith are the suggested recommendations.

1. Use LIBS to qualitatively investigate the elemental composition of the raw material used in making cosmetic powders. I also suggest that the low intensity ratio of Mg/Si and Fe/Si observed in talcum could potentially indicate the presence of asbestos. However, LIBS does not offer the means to know what the molecular structure of this. I therefore suggest that LIBS be associated with Raman spectroscopy for a comparative study of the molecular structure of talc and starch.

2. In Chapter 4 and 5, I studied the feasibility of determining the elemental composition of shales and the variation of trace elements in high-pressure CO_2-enriched water using laser-induced breakdown spectroscopy. For future research, I recommend investigating the effect of supercritical CO_2 on shale rocks in the context of carbon sequestration.

112